Landslides as geological hotspots of CO2 emission: clues from the instrumented Séchilienne landslide, western European Alps.

Pierre Nevers, Julien Bouchez, Jérôme Gaillardet, Christophe Thomazo, Delphine Charpentier, Laëticia Faure, Catherine Bertrand

▶ **To cite this version:**

Pierre Nevers, Julien Bouchez, Jérôme Gaillardet, Christophe Thomazo, Delphine Charpentier, et al.. Landslides as geological hotspots of CO2 emission: clues from the instrumented Séchilienne landslide, western European Alps.. Earth Surface Dynamics, 2021, 9 (3), pp.487-504. 10.5194/esurf-9-487-2021 . hal-03289192

HAL Id: hal-03289192
https://hal.science/hal-03289192

Submitted on 17 Jul 2021

HAL is a multi-disciplinary open access archive for the deposit and dissemination of scientific research documents, whether they are published or not. The documents may come from teaching and research institutions in France or abroad, or from public or private research centers.

L'archive ouverte pluridisciplinaire **HAL**, est destinée au dépôt et à la diffusion de documents scientifiques de niveau recherche, publiés ou non, émanant des établissements d'enseignement et de recherche français ou étrangers, des laboratoires publics ou privés.

Distributed under a Creative Commons Attribution 4.0 International License

Earth Surf. Dynam., 9, 487–504, 2021
https://doi.org/10.5194/esurf-9-487-2021
© Author(s) 2021. This work is distributed under
the Creative Commons Attribution 4.0 License.

Earth Surface Dynamics
Open Access
EGU

Landslides as geological hotspots of CO_2 emission: clues from the instrumented Séchilienne landslide, western European Alps

Pierre Nevers[1], Julien Bouchez[2], Jérôme Gaillardet[2,4], Christophe Thomazo[3], Delphine Charpentier[1], Laëticia Faure[2], and Catherine Bertrand[1]

[1]UMR Chrono-environnement, 16 Route de Gray, 25000 Besançon, France
[2]Université de Paris, Institut de physique du globe de Paris, CNRS, 75005 Paris, France
[3]UMR CNRS/uB6282 Biogéosciences, 6 Boulevard Gabriel, 21000 Dijon, France
[4]Institut Universitaire de France, 1 rue Descartes, 75231 Paris, France

Correspondence: Pierre Nevers (pierre.nevers@univ-fcomte.fr)

Received: 26 May 2020 – Discussion started: 10 June 2020
Revised: 17 March 2021 – Accepted: 30 March 2021 – Published: 3 June 2021

Abstract. This study makes use of a highly instrumented active landslide observatory (9 years of data) in the French Alps, the Séchilienne slope. Here, we use a combination of major element chemistry and isotopes ratios ($^{87}Sr/^{86}Sr$, $\delta^{34}S$) measured in different water types of the stable and unstable part of the Séchilienne instability to assess the contribution of the different lithologies of the slope and the chemical weathering mechanisms. Chemical and isotopic ratios are used to characterize weathering processes and the origin of waters and their flow paths through the massif. A mixing model allows us to allocate the different major elements to different sources, to identify secondary carbonate formation as a major process affecting solutes in the subsurface waters of the instability, and to quantify the involvement of sulfuric and carbonic acids as a source of protons.

We show that the instability creates favorable and sustained conditions for the production of sulfuric acid by pyrite oxidation, by opening new fractures and supplying fresh reactive surfaces. We clearly identify the contribution of the dissolution of each mineral phase to the chemistry of the waters, with a clear role of remote gypsum dissolution to the sulfate budget in the sampled waters. We are also able to refine the preexisting hydrogeological views on the local water circulation and water flow paths in the instability by showing the hydrological connectivity of the different zones. Overall, our results show that the Séchilienne landslide, despite its role in accelerating rock chemical and physical weathering, acts as a geological source of CO_2 to the atmosphere. If generalizable to other large instabilities in mountain ranges, this study illustrates the complex coupling between physical and chemical erosion and their impact on the carbon cycle and global climate. The study also highlights the importance of distinguishing between sulfite oxidation and gypsum dissolution as a source of sulfate ions to rivers, particularly in mountain ranges.

1 Introduction

The weathering of rocks plays a key role in the chemical and climatic evolution of the Earth surface and is one of the geological processes that impacts atmospheric CO_2 concentration. When carbonic acid is the proton supplier, silicate weathering removes carbon dioxide from the atmosphere (Lerman et al., 2007; Berner and Berner, 2012). However, the oxidative dissolution of sulfides (e.g., pyrite FeS_2) produces sulfuric acid that can act as an alternative proton supplier to chemical weathering reactions. Although not directly influencing atmospheric CO_2, silicate weathering by sulfuric acid does reduce the potential of rock weathering with respect to CO_2 sequestration by "removing" silicates from the Earth surface and, thus, limiting their weathering by carbonic acid. When sulfuric acid reacts with carbonate minerals, dissolved

inorganic carbon is added to ambient waters which leads to CO_2 release towards the atmosphere in the long term (Lerman et al., 2007; Calmels et al., 2007; Li et al., 2008; Torres et al., 2014). The relevance of this process for the global carbon cycle is two-fold. First, even though carbonate rocks do not constitute the major fraction of the rock types exposed at the Earth surface, the dissolved products of carbonate dissolution dominate global weathering fluxes (Gaillardet et al., 1999) as carbonate minerals dissolve several orders of magnitude faster than silicates (Lasaga, 1984). Second, because weathering by sulfuric acid is mainly limited by the supply of sulfide minerals to the Earth surface, it is particularly prominent in active mountain belts characterized by high erosion rates (Calmels et al., 2007; Torres et al., 2016; Blattmann et al., 2019). Within these tectonically active environments, landslides are likely to be hotspots of sulfuric acid production, carbonate weathering and CO_2 release (Emberson et al., 2015, 2018). Indeed, slope instability leads to sustained grain comminution and fractures opening, thereby providing a continuous supply of contact surfaces between water, air and minerals that can, in particular, allow for sulfuric acid production and carbonate mineral weathering (Binet et al., 2009; Bertrand et al., 2015).

Here, we explore the hypothesis that slope instability can constitute a mechanism promoting coupled sulfide oxidation and carbonate weathering, in a contribution to the study of the role active mountain ranges play on the global carbon cycle (Raymo and Ruddiman, 1992; Hilton and West, 2020). We focus on the Séchilienne slope instability located in the French Alps. This site of active, slow landsliding serves as an observatory for landslide processes and has been the subject of previous hydrogeological and geophysical investigation (Vengeon, 1998; Guglielmi et al., 2002; Meric et al., 2005; Le Roux et al., 2011; Vallet et al., 2015a; Lajaunie et al., 2019). We combine measurements of the concentration of major elements and of the isotope composition of strontium and sulfur ($^{87}Sr/^{86}Sr$, $\delta^{34}S$) dissolved in groundwater and springs to estimate the contribution of different rock types to the dissolved species produced by weathering reactions in the landslide. In particular, we estimate the relative role of different acid types (carbonic vs. sulfuric) and of two rock types (silicates vs. carbonates), and we evaluate the role played by secondary carbonate formation on the solute budget of percolating waters. Besides shedding light on the global impact of landsliding on atmospheric CO_2, Sr and S isotopes coupled to water chemistry allow for a quantitative analysis of solute sources in natural waters and of the chemical evolution of natural waters, which in turn opens the possibility to improve existing hydrogeological models in complex environments such as landslides.

2 Study area

2.1 Geological setting

The "Séchilienne" site hosts a highly instrumented, continuously monitored landslide and is part of the French National Landslide Observatory (OMIV; http://www.ano-omiv.cnrs.fr/, last access: 19 May 2021). The Séchilienne massif is located at the southwestern border of the Paleozoic crystalline Belledonne mountain range in the French Alps, 20 km southeast of Grenoble (Isère, France; Fig. 1). The active zone of the site is a gravitational instability affecting 60.10^6 m^3 of material, with a maximum depth of about 150 m, located on a south-facing slope of the massif (Le Roux et al., 2011). The most active part of the landslide, referred to as "les Ruines", is located on the eastern border of the unstable zone. Long-term monitoring (extensometers, geodetic measurements, tacheometers and microwave radar) shows that the displacement velocity is around 300 cm yr^{-1}, while the less active parts of the site are moving at a mean of 10 cm yr^{-1} (Le Roux et al., 2011; Dubois et al., 2014).

Geological and structural information is provided by the geological map and by two boreholes drilled in 2010 in the unstable area at depths down to 150 m. Baudement et al. (2013) integrated this information in a GOCAD® 3D model, recently used by Lajaunie et al. (2019) to propose a new vision of the Séchilienne slope based on a 3D resistivity model. The basement of the massif is mainly composed of mica schists showing a north–south trending subvertical foliation. Stratigraphically discordant deposits dating from the Carboniferous to the Liassic periods cover the mica schists on the top north-northeast of the massif (Mont Sec) and along the Sabot Fault (Fig. 1). The slope is locally covered by Quaternary (Würm) glaciofluvial deposits made of material reworked from the surrounding formations (Vengeon, 1998; Vallet, 2014). The mica schists consist primarily of quartz, biotite, phengite and chlorite with the occurrence of carbonate veins and pyrite in fractures. Carboniferous deposits are made of black shales, sandstones and conglomerates with quartz and serpentine pebbles. Triassic rocks correspond to sandstone, quartzite, dolomite and locally to black shales, argillites and gypsum. Liassic deposits are limestones with intercalation of layers rich in breccia consisting of mica schist, dolomite and coal (Barféty et al., 1972; Vengeon, 1998; Vallet, 2014). Strong local heterogeneities exist in terms of lithology and fracture density and are induced by the gravitational deformation (Lajaunie et al., 2019).

The part of the slope affected by the landslide extends from 400 to 1100 m above sea level (a.s.l.; Le Roux et al., 2011; Fig. 1d). Above the elevation of 1100 m a.s.l., the morphology of the Mont Sec corresponds to a plateau of glacial origin underlain by moraine deposits concentrated in small topographic depressions. The landslide is delimited at its northern border by a major head scarp of about 10 m high and several hundreds of meters wide, which separates the

glacial plateau of Mont Sec from the unstable zone. Eastward, north–south fault scarps limit the landslide, whereas the western and southern parts are not well defined by geomorphological evidence. The motion of the landslide consists of a deeply rooted, toppling movement with N50–N70 slabs toward the valley, coupled with the sagging of the upper zone of the slope near the Mont Sec (Vengeon, 1998). The Séchilienne instability is assumed to originate from the decompression of the basement rocks after the Romanche Glacier retreated at the last glaciation (15 kyr ago). Decompression caused the opening of fractures and then the collapse of the summit of Mont Sec (Montjuvent and Winistorfer, 1980; Vengeon et al., 1999; Potherat and Alfonsi, 2001). Thus, the Séchilienne slope is affected by a dense network of near-vertical, open fractures trending N70 and N110–N120 that control the deformation of the Séchilienne landslide, which is characterized by a deep progressive deformation (about 100–150 m) and the absence of a well-defined basal sliding surface. Two N20 major fractures also cross the Séchilienne massif and the Sabot and Séchilienne faults. Open fractures are locally filled with detrital material resulting from the erosion of the massif (Vallet et al., 2015a).

Borehole logs available within the instability (Lajaunie et al., 2019) show that the rock formations below the slope are relatively unstructured and that pyrite is heterogeneously distributed therein. Rock samples along the boreholes seem to have been subjected to oxidizing conditions, albeit with no clear sulfide reaction front at the scale of the instability. In addition, petrological observations on thin sections from these boreholes, combined with mineralogical analyses obtained from X-ray diffraction (XRD; Supplement, Sect. S1) show that pyrite is disseminated within the rocks, with no particular association with calcite. Gypsum was not detected from XRD analyses in the sampled rocks, consistent with results from inverse modeling by Vallet et al. (2015a), suggesting that sulfate in waters from the unstable zone (UZ) essentially originates from pyrite oxidative weathering.

2.2 Hydrogeological setting

Heterogeneous porosity and fracture density of the Séchilienne massif leads to distinct and complex patterns of hydrological flow paths. At Séchilienne, water pathways are characterized by different transit times related to a dual permeability behavior that is typical of fractured rock aquifers where conductive fractures play a major role in the drainage (Fig. 1c): rapid transit of infiltration waters through fractures reflects the functioning of a so-called "reactive" hydrological component, whereas slower transit of water through the micro-fissured, less permeable rock matrix, resulting in a smeared response of flow rate to rainfall, typifies an "inertial" circulation (Maréchal, 1998; Cappa et al., 2004; Vallet et al. 2015a). In particular, the Sabot and Séchilienne faults play an important role in fluid flow through the massif by draining waters from the sedimentary cover at a fast rate ($0.7\,km\,d^{-1}$) and bypassing the less pervious and more inertial micro-fissured matrix characterized by lower flow velocity ($0.08\,km\,d^{-1}$) (Mudry and Etievant, 2007; Vallet et al., 2015a). Local perched aquifers develop during high-flow periods and discharge downwards to the main aquifer due to the contrast in permeability between the decompressed zone at the surface and the unaltered rock (Lajaunie et al., 2019). An underground tunnel for the production of electricity in a local hydropower plant, named "Galerie EDF", built by Electricité de France (EDF) and located at the base of the slope, acts as a major westward drain for groundwater (Vallet et al., 2015a).

The difference in hydraulic conductivity between the highly fractured unstable zone (thickness of about 150–200 m; Le Roux et al., 2011) and the basement situated under the landslide (Fig. 1d) led to the buildup of a two-layer aquifer system. These two layers are connected to one another through major fractures (Vengeon, 1998; Meric et al., 2005; Le Roux et al., 2011; Guglielmi et al., 2002; Vallet et al., 2015a). A temporary and discontinuous shallow perched aquifer is present in the landslide with extension and connectivity varying according to short-term recharge variations. This aquifer is almost dry during the low-flow periods, with numerous disconnected saturated pockets (such as open fractures filled by colluvial deposit and altered material) linked to the heterogeneity of the landslide (Guglielmi, 2002; Cappa et al., 2004; Vallet et al., 2015a). The recharge of this aquifer is mainly local (through trenches and counterscarps, limiting the runoff) with a contribution from remote groundwater through near-surface drainage during high-flow periods from the sedimentary cover above the landslide (near the Mont Sec summit) (Guglielmi, 2002; Vallet et al., 2015a). The deep aquifer, which extends throughout the massif (altitude around 550 m a.s.l.), corresponds to a saturated layer hosted by the fractured metamorphic bedrock and to an overlying, 100 m thick vadose layer (Vallet et al., 2015a). The deep aquifer level is controlled by the constant water heads of the Romanche alluvium in the valley and of the Galerie EDF (425 m a.s.l.).

3 Samples and analytical methods

Nine outflows draining the whole massif were investigated for physicochemical parameters and dissolved load chemistry (Fig 1.a). Two of these outflows (G1 and G2) are located within the unstable zone (UZ) and correspond to seep water collected in a tunnel excavated to monitor the landslide at 710 m a.s.l. (G710). The remaining outflows (S10, S12, S13, S15, S18, S20 and S21) correspond to springs draining the stable zone (Fig. 1b). These outflows can be differentiated by the dominant local lithology: S10 is located in the bedrock stable zone (BSZ), S12 is located in the carbonate stable zone (CSZ), and S13, S15, S18, S20, and S21 are located in an area of the stable zone characterized by mixed

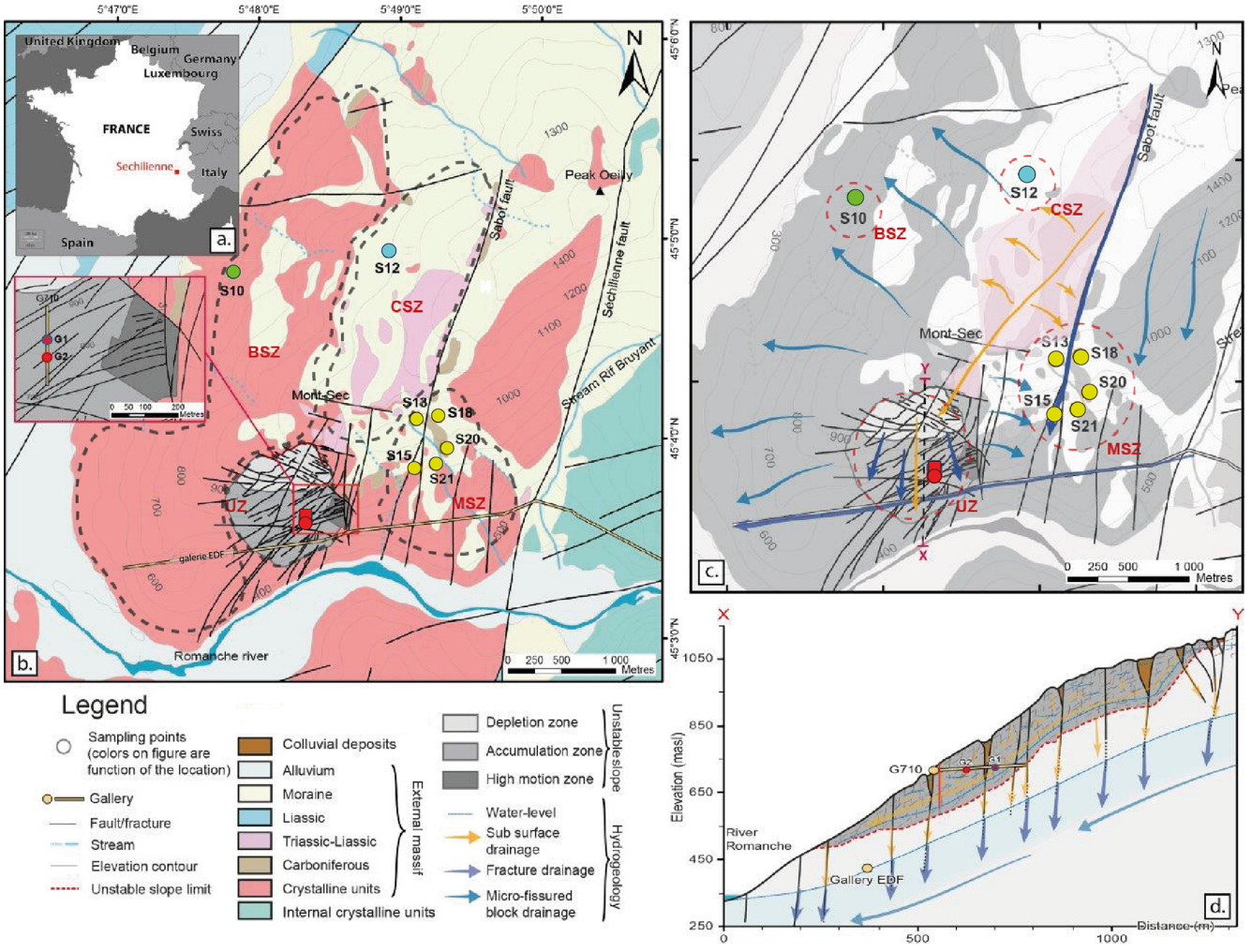

Figure 1. **(a)** Map of the Séchilienne site. **(b)** Location of the Séchilienne massif in the French Alps. **(c)** Simplified geological map of the Séchilienne massif and sampling locations. **(d)** Schematic hydrogeological model of the Séchilienne massif. Hydrogeological cross section of the instability, modified after Vallet et al. (2015).

lithology (mixed stable zone, MSZ). Samples were collected every 3 months over the period from 2010 to 2019. Between 2014 and 2017, waters were sampled once a year for Sr isotopes; samples for S isotope were collected in 2019. In total, 360 water samples were collected and analyzed for this study. Four local rocks samples were taken, reflecting the main lithological types encountered at Séchilienne: basement mica schist, carbonate (both calcite-rich and dolomite-rich) from the sedimentary cover, and a recrystallized vein in mica schist.

Field measurements of water temperature, pH and electrical conductivity (EC) were made with a WTW pH/Cond 340i (Xylem Inc.) sensor, with a precision of 0.1 unit and 0.1 µS cm^{-1} for pH and EC, respectively. Water samples were collected in polyethylene bottles and filtered with a 0.45 µm pore diameter nylon filter before being preserved under cold conditions for the measurement of major element concentration and Sr and S isotopes. Analyses of dissolved major elements were all carried out at the Chrono-Environnement research laboratory at the University of Franche-Comté. Dissolved major cation concentrations were measured by atomic absorption spectrometry (AA 100 PerkinElmer) with detection limits of 0.5, 0.1, 0.01 and 0.1 mg L^{-1} for Ca^{2+}, Mg^{2+}, Na^{+} and K^{+}, respectively. Dissolved anion concentrations were determined using high-pressure ion chromatography (Dionex DX 100) with detection limits of 0.1, 0.1 and 0.05 mg L^{-1} for Cl^{-}, SO_4^{2-} and NO_3^{-}, respectively. The concentration of HCO_3^{-} was measured by acid titration (N/50 H_2SO_4) within 48 h of sampling, with 1 % accuracy. The dissolved silica concentration was analyzed with a spectrophotometer (Spectroquant, Pharo 300, Merck) using a silica-test kit (Merck) with 3 % accuracy. Only analyses with a charge balance better than 10 % were taken into account.

Strontium isotope analyses were carried out at the High-Resolution Analytical Platform (PARI) of the Institut de Physique du Globe de Paris (IPGP). For water samples, dissolved Sr was first isolated from the water sample matrix by automated ion chromatography following the method of Meynadier et al. (2006). For rocks, in addition to bulk sample analysis after digestion in concentrated HF and HNO_3, a three-step sequential leaching procedure was conducted using H_2O, 1M acetic acid and 1M HCl. The first step was designed to recover the exchangeable fraction adsorbed onto the solid surface; step 2 was for extracting Sr from carbonates, amorphous hydroxides and phosphate minerals (Tessier et al., 1979); step 3 was to dissolve any high-order Fe–Mn oxide/oxyhydroxide phases that might be present after HCl leaching (Tessier et al., 1979). The leachate solutions and residual samples were measured for major and trace elements using a Quadrupole Inductively Coupled Plasma Mass Spectrometer (ICP-MS; Agilent 7900) with a precision better than 5 % and were processed for $^{87}Sr / ^{86}Sr$ ratio analysis following the same procedure used for bulk samples. To that effect, 3M HNO_3 aliquots of digestion solutions were loaded on columns loaded with 0.2 mL of Sr-SPEC resin (Eichrom). Next, 3M HNO_3 was used to elute the sample matrix before Sr was eluted in H_2O. Strontium isotope ratios were then measured using a Multi-Collector Inductively Coupled Plasma Mass Spectrometer (MC-ICP-MS; Thermo Scientific Neptune) in low-resolution mode (Hajj et al., 2017). Purified Sr solutions were introduced using an APEX desolvation unit and a PFA nebulizer at a rate of 50 to 100 µL min^{-1}, depending on the measurement session, and at Sr concentrations between 50 and 150 ppb. The accuracy and reproducibility of the $^{87}Sr / ^{86}Sr$ analysis was assessed using repeated measurements of the international isotope Sr carbonate standard (SRM987, NIST). Over three sessions of measurements, the average value for SRM987 standard NIST was 0.710249 ± 0.000025, which is in agreement with the accepted value.

Sulfur isotope measurements were performed at the Biogéosciences Laboratory, University of Burgundy, Dijon, France, on both sulfates from water samples and sulfides from basement mica schist. Nine samples were treated with an excess of 250 g L^{-1} $BaCl_2$ solution to precipitate $BaSO_4$. After centrifugation, the $BaSO_4$ precipitate was washed several times with deionized distilled water and dried at 60 °C for 24 h in an oven. A total of 500 µg of the respective purified barite samples was poured into tin capsules and homogeneously mixed with one-third of vanadium pentoxide before isotopic measurements (^{34}S, ^{32}S) using a vario PYRO cube (Elementar GmbH) connected online via an open-split device to an IsoPrime IRMS system (Isoprime, Manchester, UK). Sulfur isotope data are expressed in δ notation and reported in per mill (‰). The $\delta^{34}S$ data are reported with respect to the international Vienna Canyon Diablo Troilite (VCDT) standard. Analytical errors are ± 0.3 ‰ (1σ) based on replicate analyses of the NBS-127 international barite standard, which was used for data correction assuming a $\delta^{34}S$ value of +20.3 on the VCDT scale.

Sulfur contained in sulfides was extracted from eight rock samples of the basement mica schist formation in 3 g aliquots (four subsamples of each of two rock samples, including unaltered pyrite and iron oxides) following the method described by Canfield et al. (1986). Dried and rinsed Ag_2S precipitates recovered after wet chemistry sulfide extraction were weighted for gravimetric quantification of sample sulfur content. A total of 500 µg of silver sulfide precipitates was then mixed with an equivalent weight of tungsten trioxide in tin capsules before combustion in a vario PYRO cube (Elementar GmbH). Sulfur isotope compositions ($\delta^{34}S$) were measured using an IsoPrime IRMS device (Isoprime, Manchester, UK). International standards (IAEA-S-1, IAEA-S-2 and IAEA-S-3) were used for calibration, and the results are reported in δ notation relative to the Vienna Canyon Diablo Troilite (VCDT) standard. Reproducibility (1σ) is better than 0.2 ‰ based on duplicate analyses of standard materials and samples.

4 Results

The concentration of major and trace elements as well as the Sr and S isotope composition of rock samples are given in Tables 1 and 2 (data available at https://doi.org/10.5281/zenodo.4606732). The concentration of major elements, EC, pH, temperature, and the Sr and S isotope composition of water samples are given in Table 3.

4.1 Major elements

4.1.1 Rock samples

The two limestone samples show a distinctive response to the leaching procedure, with most of the Ca of the "Laffrey" limestone located in the acetic acid leachate (67 %) and the rest in the HCl fraction (11 %), which is indicative of the calcitic nature of this rock sample (Table 1). By contrast, most of the Ca of the "Lias" sample is hosted in the residue, while a significant fraction (37 %) is HCl-soluble, suggesting that the carbonate fraction of this sample is dolomitic. The "mica schist" and "vein" samples have higher bulk Sr / Ca, Mg / Ca, Al / Ca and Na / Ca ratios than the two limestone samples, confirming that they are mostly made of silicate minerals.

4.1.2 Spring water samples

The chemical composition of waters sampled at the Séchilienne site is very diverse, reflecting heterogeneity in rock types and the existence of various groundwater flow paths. Water pH at Séchilienne is relatively high and varies from 6.5 to 9.4 with a mean value of 7.9. Electrical conductivity ranges between 79 and 1114 µS cm^{-1} (Table 3). From the

major ion perspective, samples can be grouped into four main water types (Fig. 2). These water types correspond to those identified previously by Vallet et al. (2015a). Type 1 indicates Ca–HCO_3 waters, typical of water draining carbonate formations, typified by the S12 spring draining the carbonate cover at the top of the Séchilienne slope (CSZ). S12 has low EC values ranging from 79 to 147 µS cm^{-1} with a mean of 117 µS cm^{-1}. The second group corresponds to Mg–Ca–HCO_3-rich waters, which have circulated through the sedimentary cover (carbonate and dolomite) and the mica schists bedrock, and is represented by the S10 spring (BSZ). All S10 samples have higher electrical conductivities ranging from to 308 to 509 µS cm^{-1} with a mean of 443 µS cm^{-1}. Waters sampled in the unstable part of the slope (UZ) include the G1 and G2 underground outflows, show a chemical composition that varies from Mg–Ca–HCO_3–SO_4 waters to Mg–Ca–SO_4 waters and constitute the third hydrogeochemical group. The highest EC values in this study are observed for the G1 outflow with electrical resistivities ranging from 613 to 1114 µS cm^{-1} and a mean value of 824 µS cm^{-1}. The other outflow of the unstable zone (outflow G2), in contrast to the previous one, shows a mean electrical conductivity value of around 391 µS cm^{-1}, with a minimum value of 313 µS cm^{-1} (and a maximum value of 470 µS cm^{-1}). The fourth and last type of waters include the S13, S15, S18, S20 and S21 outflows, sampled in the stable part of the slope (MSZ) along the Sabot Fault, and show Ca–Mg–HCO_3–SO_4-type waters. The MSZ group exhibits EC values ranging from 357 to 567 µS cm^{-1}, with a mean of 479 µS cm^{-1}. Waters of the unstable zone group (G1, G2) are characterized by the highest concentrations of SO_4^{2-} (from 1.32 to 3.90 mmol L^{-1}) compared with the other outflows sampled which have values ranging from 0.57 to 1.34 mmol L^{-1} for the MSZ outflows (S13, S15, S18, S20 and S21) and from 0.48 to 0.67 for the S10 (BSZ) outflow (Fig. 2; Table 3). Figure 2 clearly shows that SO_4^{2-} ions significantly contribute to the electrical balance of the analyzed waters. Dissolved Cl^- concentrations are lower than 50 µmol L^{-1} in the S10, S12, S13 and S18 springs but can reach values above 100 µmol L^{-1} in the S15, S20 and S21 springs. Dissolved NO_3^- concentrations are typically below 20 µmol L^{-1} in the G1, G2 and S10 springs but are higher in the S12, S13, S18, S15, S20 and S21 springs, with concentrations above 100 µmol L^{-1} observed in the latter group (Table 3).

Rainwater samples (Table 3) show very low EC values with a mean of 26 µS cm^{-1} and low concentrations for all elements analyzed. In particular, chloride concentrations range from 3.3 µmol L^{-1} to 20.3 µmol L^{-1}.

4.2 Strontium isotopes

4.2.1 Rock samples

The two carbonate rock samples have the lowest Sr isotopic ratios (Table 1), with the lowest value of 0.7095

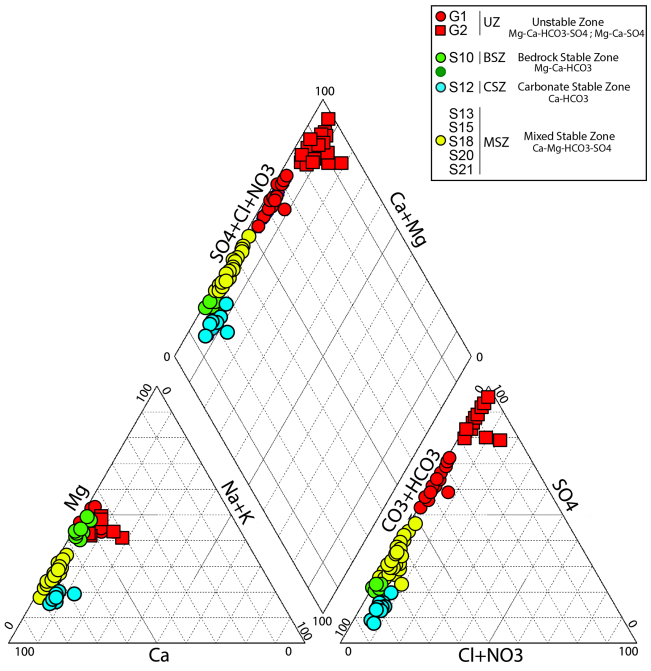

Figure 2. Piper diagram representing the major water types sampled in the outflows of the Séchilienne massif.

being slightly higher than the Sr isotopic composition of lower Jurassic seawater (from 0.7065 to 0.7076; Koepnick et al., 1990). The acetic-acid- and HCl-soluble fractions of the limestone samples, as well as the bulk analysis of the dolomitic Lias sample and its H_2O leachate, are characterized by $^{87}Sr/^{86}Sr$ ratios of ~ 0.7105. The $^{87}Sr/^{86}Sr$ ratio of all the leachates of the calcitic Laffrey sample, as well as of the bulk sample, show a wider range of variation, in the range from 0.7104 to 0.7179. By contrast, the highest $^{87}Sr/^{86}Sr$ ratios were found in the mica schist samples with a value of 0.7351 (Table 1), which is typical of silicate rocks (0.73 ± 0.01; Négrel et al., 1993). The veins contained in the mica schists also show high Sr isotopic ratios (0.7277). Such high $^{87}Sr/^{86}Sr$ ratios are particularly encountered in the residues and bulk samples.

4.2.2 Spring water samples

The Sr isotope ratios measured in the spring samples in and around the Séchilienne instability range from 0.7093 to 0.7231 (Table 3). The four main groups of waters have contrasted $^{87}Sr/^{86}Sr$ isotopic ratios. The highest $^{87}Sr/^{86}Sr$ values are found in the UZ underground outflows samples (G1, G2) with an average of 0.7210 ± 0.0006 (1 standard deviation). The lowest $^{87}Sr/^{86}Sr$ values correspond to the waters of the MSZ (springs S13, S15, S18, S20 and S21) and average at 0.7095 ± 0.00012, i.e., at the value measured in the carbonate rock. The S12 outflow (CSZ) is characterized by $^{87}Sr/^{86}Sr$ ratios of around 0.7095 ± 0.00005, i.e., close to those of the MSZ group. Intermediate values of Sr isotopic

ratios are found for the samples of the BSZ group (S10), with an average of 0.7148 ± 0.00019.

4.3 Sulfur isotopes

4.3.1 Rock samples

The sulfur isotope composition of unaltered rock samples (four samples) range from -7.9 ‰ to 17.8 ‰ with an average value of $1.2‰ \pm 11.8‰$, whereas weathered mica schists (four samples) exhibit $\delta^{34}S$ values ranging from -13.1 ‰ to 9.9 ‰ and an average of $-1.4‰ \pm 9.5‰$; (Table 2). These numbers show the extremely large range of possible sulfur isotope signals coexisting in the various rock types present in the landslide.

4.3.2 Spring water samples

Waters show a much narrower range of $\delta^{34}S$ values, ranging from -5.5 ‰ to 6.5 ‰ (mean $0.43‰ \pm 5.12‰$). The highest $\delta^{34}S$ values are observed for water of the MSZ group (outflows S13, S15, S20 and S21) with an average of $6.28‰ \pm 0.34‰$. Samples of the S12 outflow (CSZ group) also exhibit a high $\delta^{34}S$ value of 6.03 ‰. The G1 and G2 outflows (UZ group) exhibit negative $\delta^{34}S$ values with an average of $-3.74‰ \pm 1.75‰$, with lower $\delta^{34}S$ values for G2 (averaging at $-5.33‰ \pm 0.22‰$) than for G1 ($2.2‰ \pm 0.06‰$). The BSZ group (outflow S10) is characterized by $\delta^{34}S$ values that are intermediate between those of the MSZ and UZ groups (2.4 ‰).

5 Discussion

5.1 Identification of sources of dissolved species

5.1.1 Atmospheric and anthropogenic sources

Rainwater is potentially a significant source of elements for the water sampled in the different springs at Séchilienne. To assess the importance of atmospheric inputs, we use Cl^- concentrations. Chloride is not significantly involved in chemical reactions at the Earth surface, and its presence in waters has three main origins: rainwater (through the dissolution of sea salt aerosols), dissolution of saline rocks or inclusions, and anthropogenic inputs. On the other hand, at Séchilienne, NO_3^- is most likely to be derived from human activity, through fertilizer input and/or domestic waste. Therefore, the correlation between Cl^- and NO_3^- concentrations in the S15, S20 and S21 springs ($R^2 = 0.65$; Fig. S8 in the Supplement) suggests that, beyond rainwater, anthropogenic inputs are a significant Cl^- source to these springs. This inference is consistent with the presence of villages upslope from these springs. High Cl^- concentrations ($> 100\,\mu mol\,L^{-1}$) are also found in some samples from the G1 and G2 underground outflows (Table 3). However, in the case of these two springs, such high Cl^- concentrations are not accompanied by high NO_3^- concentrations but correlate to some extent with dissolved Na^+ and K^+ concentrations (Fig. S8). This observation could be indicative of the dissolution of salts (NaCl and KCl) as a significant process delivering Cl^- and cations to the springs. Although the origin of these salts is unclear, we note that Zn–Pb ore deposits are reported in the bedrock of Séchilienne landslide exploitation (Barnes, 1997). The presence of fluid inclusions containing alkali elements and Cl in these ores is likely, and leaching of such fluid inclusions could have occurred because of the exposure of new mineral surface during ore extraction. To summarize, the excess of Cl in Séchilienne springs is most probably due to a combination of human activity (road salts and agriculture) and to the dissolution of fluid inclusions of hydrothermal origin.

The expected concentration of Cl^- derived from precipitation in spring waters (hereafter called $[Cl]_{crit}$ for "critical chloride"; Stallard et al., 1983) of the Séchilienne massif can be estimated by multiplying the mean Cl^- concentration found in rainwater by the mean evapotranspiration factor (P / ETP: 4.02, with P, precipitation, and ETP, evapotranspiration, calculated from the temperature and latitude of the study site, according to Oudin et al., 2005). Alternatively, $[Cl]_{crit}$ can be estimated as being equal to the lowest Cl^- concentrations in the sample set (S10, S12 and S21 springs). Both methods concur to fix the atmospheric contribution of Cl^- to the Séchilienne waters at a maximum of $30\,\mu mol\,L^{-1}$. Above this concentration, additional sources must be involved. Once $[Cl]_{crit}$ is known, it is possible to correct all cation concentrations from the atmospheric sea salt input using

$$[X]^* = [X] - [Cl]_{crit} \times \left(\frac{X}{Cl}\right)_{seawater}. \quad (1)$$

In this equation, $[X]^*$ denotes the concentration of an element X in the water sample, corrected from the atmospheric input, and $(X / Cl)_{seawater}$ is the seawater elemental ratio. This correction is only significant for Na^+, due to the relatively high concentrations found in the Séchilienne waters.

As explained above, a significant excess of Cl^- ($[Cl] > [Cl]_{crit}$) is found for the S15, S20 and S21 springs, where this excess is the highest (about 30 to $60\,\mu mol\,L^{-1}$) due to domestic and/or agricultural activity, and in the G1 and G2 underground outflows (between 15 and $20\,\mu mol\,L^{-1}$ of excess), where this excess can be attributed to salt dissolution. For the first group of springs, it is most likely that the input of Cl^- is associated with the input of K^+, through the use of fertilizers. For the second group of springs, each mole of Cl^- released by salt dissolution can be associated with 1 mol of K^+ or 1 mol of Na^+. Because of the challenge associated with assessing the exact cause of the observed Cl^- excess in these springs, we use a stochastic approach in the quantitative source apportionment (Sect. 5.1.4) to reflect the uncertainty linked to the nature of the cations delivered to the springs by these Cl^- sources. However, we emphasize that

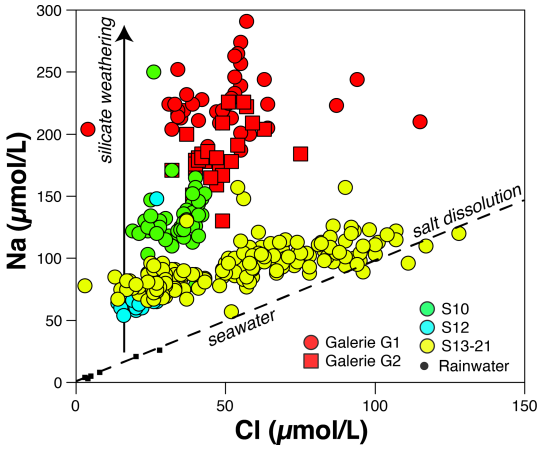

Figure 3. Na vs. Cl concentrations measured in the different groups of water outflow from the Séchilienne massif. Rainwater data points are aligned along the seawater composition (sea salts).

for the springs where silicate weathering is the most prominent process in terms of cation production (G1 and G2; see Sect. 5.1.2 below), the correction for the solute sources causing the Cl^- excess (human activity and salt dissolution) is relatively minor.

5.1.2 The importance of silicate weathering

The concentration of Na^+, once corrected from atmospheric and anthropogenic inputs, can be used as a proxy of silicate weathering reactions if the dissolution of silicate minerals is a dominant source of Na to surface waters compared with salt dissolution and human activity. The G1 and G2 underground outflows have the highest Na* concentrations (mean values of 200 ± 30 and $158 \pm 21\,\mu mol\,L^{-1}$ for G1 and G2, respectively) (Fig. 3). This observation suggests the importance of silicate weathering reactions in the unstable zone, which is made of fractured mica schists. Although, as explained above, the source of excess chloride could also be contributing Na (were this additional source NaCl inclusions), the Na* concentrations remain the highest found in the Séchilienne landslide area assuming that all Cl^- release to waters is associated with an equivalent Na^+ release (in moles). Despite their excess of Cl^-, the MSZ outflows' chemistry also reveals that silicate weathering reactions are releasing Na^+ to those waters (Fig. 3). However, the Na* concentrations of the mixed stable zone ($60\,\mu mol\,L^{-1}$ on average) are equal to around half of those encountered in the unstable zone. This contrast between the stable (MSZ) and unstable (UZ) zones illustrates that the intensity of silicate weathering is linked to the degree of fracture density at Séchilienne. Finally, the low Na* concentration in the S12 outflow (Fig. 3) can be attributed to the fact that it mainly drains the carbonate cover. The most plausible explanation for the nonzero Na* concentration in S12 is the release of Na from silicate material disseminated in the carbonate rocks and/or the presence of anthropogenic inputs.

5.1.3 Identifying sources of solutes in the springs of the Séchilienne massif

In the following, we use dissolved elemental and isotopic ratios to quantitatively constrain the contribution of various rock sources (silicates, carbonates and gypsum) with respect to solutes in the Séchilienne springs. As shown above, strong contrasts exist in $^{87}Sr/^{86}Sr$ ratios between the sedimentary carbonate cover and the crystalline rocks of the basement. The isotopic ratio of dissolved Sr released by water–rock interaction reflects that of the minerals undergoing dissolution and is not affected by the reincorporation of Sr in secondary minerals (e.g., Négrel et al., 1993). Thus, Sr isotopes can be used to trace the provenance of dissolved Sr and, by extension, of the different cations in the waters of Séchilienne. By contrast, elemental ratios such as Ca / Sr and Mg / Sr may be affected by the precipitation of secondary minerals and, in particular, by the formation of secondary carbonates (Bickle et al., 2015); thus, they should be used more carefully to identify the provenance of cations.

A series of plots using $^{87}Sr/^{86}Sr$ as a common y axis are shown in Fig. 4. In $^{87}Sr/^{86}Sr$ vs. Ca / Sr or Na / Sr plots (Fig. 4a, b), conservative mixing between reservoirs is indicated by straight lines joining the end members. In this set of figures, the Ca / Sr ratios for the carbonate, silicate and evaporite end members are taken from Négrel et al. (1993) and Gaillardet et al. (1997). The corresponding Sr isotopic ratios are those measured in the rock samples from the Séchilienne massif (Table 3).

The position of the data points corresponding to springs S13, S15, S18, S20 and S21 (MSZ group) in Fig. 4a and b shows that their relatively low Sr isotopic composition cannot only be derived from the dissolution of carbonates. Another unradiogenic end member with low Ca / Sr and Na / Sr ratios needs to be invoked. As indicated by Fig. 4c, this end member is enriched in sulfate, as shown by its high SO_4 / Na ratio. Although gypsum outcrops are not visible at Séchilienne, gypsum is known to exist in the local Triassic formations present in the upper part of the slope, as indicated by the regional geological map (Fig. 1). More generally, the presence of gypsum is well documented in the Triassic strata of the "external Alps" where it plays a major role in large-scale deformation and thrusting (Barféty et al., 1972). The occurrence of gypsum and carbonate dissolution inferred from the chemistry of the Séchilienne springs indicates that the Sabot Fault, which lies northeast of the MSZ outflows (Barféty et al., 1972), plays a major role in draining aquifers hosted by sedimentary rocks to the MSZ and BSZ outflows. The Sr and S isotope composition of Triassic seawater (between 0.7075 and 0.708 and 15 ± 3 ‰, respectively; Burke et al., 1982; Fanlo and Aroya, 1998; Kampschutte and Strauss, 2004) and the typical Ca / Sr ratio of waters draining gypsum (Gail-

lardet et al., 1997; Meybeck et al., 1986) are consistent with the contribution of gypsum dissolution.

Fig. 4 also shows that the S12 spring, reported by Vallet et al. (2015a) to be supplied by rapid flow paths through the sedimentary cover, in addition to being solute-poor compared with springs of the MSZ group, is not influenced by gypsum dissolution despite its geographical position in the sedimentary part of the slope. The relatively high Na / Sr ratios observed in the S12 spring are probably due to anthropogenic influence, as revealed by the high nitrate concentrations measured in this spring (Sect. 5.1.1 and Fig. S8c).

By contrast, $^{87}Sr / ^{86}Sr$ and chemical ratios of waters from the UZ outflows (G1, G2) are clearly influenced by a silicate end member. However, their Sr isotopic signature is lower than those of the local mica schist, indicating the additional contribution of Sr from a carbonate and/or evaporitic source to the G1 and G2 spring (Fig. 4a). The $^{87}Sr / ^{86}Sr$ ratios of waters of the S10 outflow also exhibit intermediate values between the silicate and carbonate–gypsum mixing line but with a $^{87}Sr / ^{86}Sr$ ratio lower than those of the UZ outflows, supporting the idea that water–silicate interaction in the BSZ are less intense than in the UZ. These inferences based on Sr isotopes are in full agreement with those made above based on Na* concentrations and can be interpreted as reflecting the lesser degree of fracture density of the stable zone compared with the unstable zone. Figure 4c and d show that the higher $^{87}Sr / ^{86}Sr$ ratios observed in springs of the UZ (G1, G2), and to a lesser extent of the BSZ (S10), are associated with sulfate enrichment. However, unlike for samples of the MSZ (S13–S21), dissolved sulfate in UZ and BSZ samples has a relatively low S isotope composition (Fig. 4d). This observation is compatible with a significant influence of sulfide oxidation, despite the very wide range of $\delta^{34}S$ values measured in the bedrock mica schists (between $-13.14‰$ and $17.77‰$, with an average of $-0.10‰$ and SD of 10.05; Table 2).

The presence of pyrite has been reported in the unstable zone of Séchilienne (Bertrand et al., 2015; Vallet et al., 2015a). The concomitant increase in SO_4^{2-} and radiogenic Sr (Fig. 4c) combined with the decrease in $\delta^{34}S$ (Fig. 4d) suggests a coupling between sulfide oxidation and silicate weathering in the unstable zone. Indeed, the oxidative weathering of pyrite, possibly by O_2 or water, leads to the release of sulfate to waters (e.g., Spence and Telmer, 2005):

$$2FeS_2 + \frac{15}{2}O_2 + 7H_2O \rightarrow 2Fe(OH)_3 + 4H_2SO_4 \quad (2)$$

$$FeS_2 + 14Fe^{3+} + 8H_2O \rightarrow 15Fe^{2+} + 2SO_4^{2-} + 16H^+. \quad (3)$$

The oxidation of sulfide to intermediate sulfur species or to sulfate appears to produce only small isotope effects (Fry et al., 1986, 1988; Zerkle et al., 2009; Balci et al., 2012). The significance of these reactions in the unstable zone of Séchilienne can be related to the role of fracturation and grain comminution in favoring the contact between water, air and minerals, which is the rate-limiting factor for a fast chemical reaction such as pyrite oxidation.

Altogether, our analyses shows that the composition of the water outflows from the Séchilienne site can be interpreted by a variable contribution of waters having interacted with mica schists and sedimentary rocks, and by a dual origin (sulfide oxidation vs. gypsum dissolution) of sulfate ions. The chemical and isotopic characteristics of the MSZ and UZ waters show that these waters have percolated through the sedimentary cover before reaching their outlet in the massif through the Sabot Fault.

5.1.4 Quantitative apportionment

Spring dissolved Sr isotopes and major element chemistry make it possible to estimate the relative contribution of each identified end member to the different cations. The details of these calculations and results are given in the Supplement. Following the above discussion, mixing equations can be written for the conservative trace element Sr:

$$\left(\frac{^{87}Sr}{^{86}Sr}\right)_{mix} = X_{sil}^{Sr} \cdot \left(\frac{^{87}Sr}{^{86}Sr}\right)_{sil} + X_{carb}^{Sr} \cdot \left(\frac{^{87}Sr}{^{86}Sr}\right)_{carb} + X_{gyps}^{Sr}\left(\frac{^{87}Sr}{^{86}Sr}\right)_{gyps} \quad (4)$$

$$\left(\frac{Na}{Sr}\right)_{mix} = X_{sil}^{Sr} \cdot \left(\frac{Na}{Sr}\right)_{sil} + X_{carb}^{Sr} \cdot \left(\frac{Na}{Sr}\right)_{carb} + X_{gyps}^{Sr}\left(\frac{Na}{Sr}\right)_{gyps} \quad (5)$$

$$1 = X_{sil}^{Sr} + X_{carb}^{Sr} + X_{gyps}^{Sr}, \quad (6)$$

where the subscripts mix, sil, carb and gyps denote the mixture (water) and the silicate, carbonate and gypsum end members, respectively. Proportions of Sr derived from each of those end members i are denoted X_i^{Sr}. All ratios are corrected from atmospheric and salt inputs according to the above method. Because the carbonate and gypsum end members add relatively few Na compared with Na* (Na from silicates), Eq. (5) simplifies to

$$\left(\frac{Na}{Sr}\right)_{mix} = X_{sil}^{Sr} \cdot \left(\frac{Na}{Sr}\right)_{sil}. \quad (7)$$

This assumption is supported by the positions of the different springs in Fig. 4a, which indicates that the low-$^{87}Sr / ^{86}Sr$ component of the springs – encompassing both carbonate and gypsum weathering – has a negligible Na content. The proportions of Sr in the different mixing reservoirs can then be estimated, and the contribution of each of these end members to the load of the dissolved major species SO_4^{2-} and Mg^{2+} is calculated as follows:

$$X_i^E = X_i^{Sr}\left(\frac{E}{Sr}\right)_i \Big/ \left(\frac{E}{Sr}\right)_{spring}, \quad (8)$$

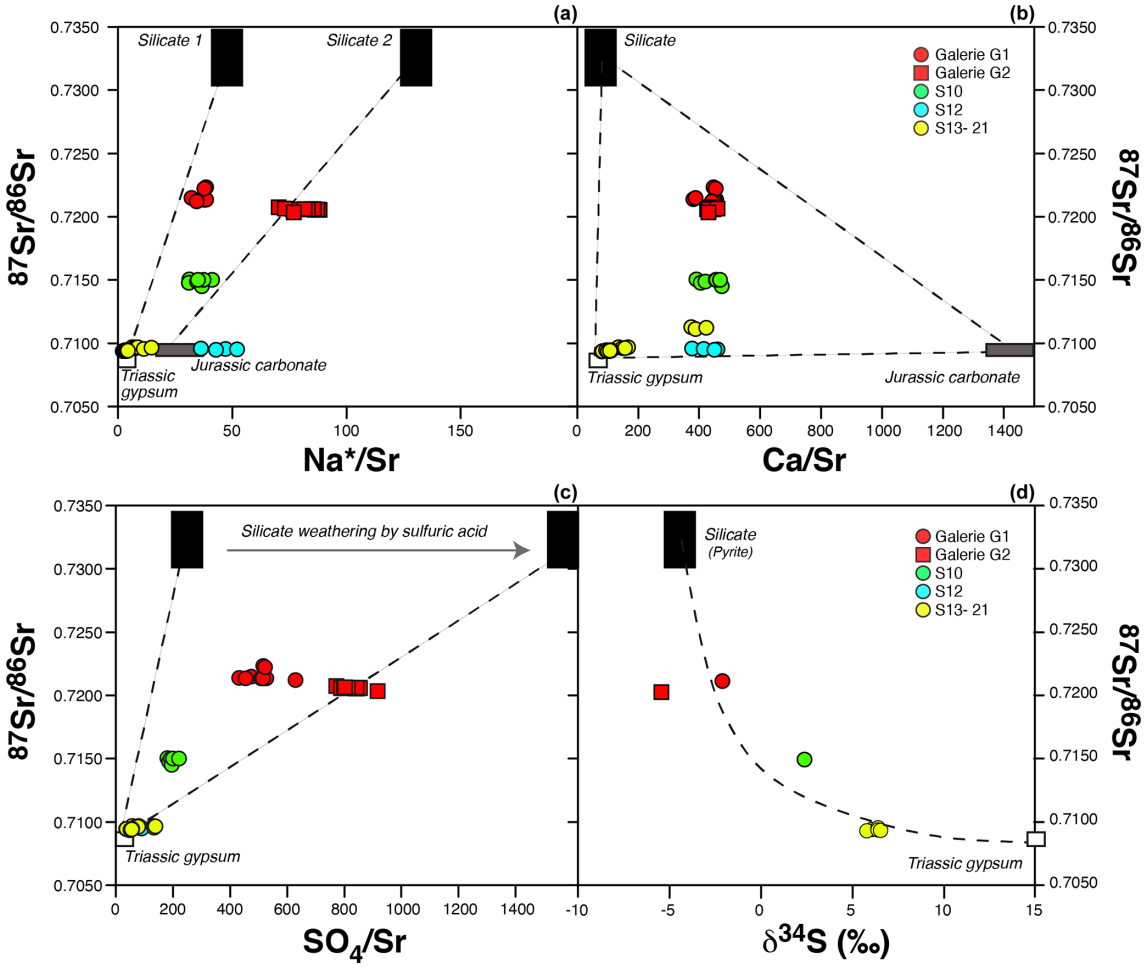

Figure 4. Sr isotopic composition of the different groups of water outflows from the Séchilienne massif as a function of Sr-normalized ratios **(a, b, c)** and S isotopic composition **(d)**. Mixing end members are discussed in the text. Straight lines indicate a mixing process in panels **(a)**, **(b)** and **(c)**. In panel **(d)**, the dashed line is a mixing hyperbola calculated based on the composition of the end members ($^{87}Sr / {}^{86}Sr$, $\delta^{34}S$ and SO_4 / Sr ratios of the silicate and carbonate end members).

with $i =$ sil, carb or gyp, and $E = SO_4$ or Mg (corrected from rain inputs. A full discussion is given in the Supplement (Sect. S3) on the choice of the $(Na / Sr)_{sil}$ (Eq. 7) and more generally of the $(E / Sr)_i$ ratios (Eq. 8), based on regression of the spring hydrochemical data and independent constraints from our geochemical analyses of the rock samples.

In carbonate-rich contexts like that of Séchilienne, dissolved Ca^{2+} concentrations can be affected by precipitation of secondary carbonates which tend to scavenge significant amounts of dissolved Ca relative to Mg and Sr (Bickle et al., 2015). For this reason, in principle, Eq. (8) cannot be applied for $E =$ Ca and $i =$ carb. The relatively high Mg / Ca ratios (around 0.9 mol/mol in the G1, G2 and S10 springs and 0.2–0.4 mol/mol in the S10–S21 springs; Table 3) and Sr/Ca ratios (around 2 mmol/mol in the G1, G2, S10, S12 and S18 springs and above 6 mmol/mol for the S13, S15, S20 and S21 springs) compared with the estimated Mg / Ca and Sr / Ca ratios of the calcite end member at Séchilienne (below 0.1 mol/mol and 1 mmol/mol, respectively) determined from our geochemical analyses of rock samples (Table 1) are indeed suggestive of a significant role of secondary carbonate formation. We quantify the role of secondary carbonate formation using the method proposed by Bickle et al. (2015), which is based on the comparison in the Sr–Ca–Mg–Na compositional space between the measurements made in springs and the prediction from conservative mixing between the rock end members (Sect. S3). In this analysis, we contend that secondary carbonate formation affects waters containing solutes derived from the three rock end members identified for the Séchilienne springs (silicates, carbonates and gypsum) after they mix. We estimate that along the water flow path secondary carbonate formation scavenges around 60 % of the Ca initially released to solution by the combined dissolution of silicates, carbonates and gypsum for the G1, G2, and S10 springs, whereas the effect of secondary carbonate precipitation is negligible for the other springs (Sect. S3).

These results highlight the potential role of lithological diversity, a characteristic of the bedrock material drained by the G1, G2 and S10 springs in the UZ and BSZ (compared with other springs mostly influenced by the carbonate cover), in promoting secondary carbonate formation through mixing of compositionally different waters.

Another challenge in using Eq. (8) at Séchilienne is the fact that both calcite and dolomite are reported to occur as carbonate minerals at Séchilienne – as confirmed by our own chemical analyses of rock samples (Table 1). Therefore, we take the presence of dolomite into account in our quantitative source apportionment, in particular regarding the $(Mg / Sr)_{carb}$ ratio used in Eq. (8) (Sect. S3). Based on arguments linked to the extent of secondary carbonate precipitation needed to explain the spring data (see above), we estimate that the contribution of dolomite dissolution to the overall Ca released by carbonate weathering at Séchilienne is about 10 % to 20 % (Supplement).

In order to quantify the uncertainty associated with our mixing model, a Monte Carlo approach was used with 10 000 simulations. Results are given in Table S2 (in the Supplement) and represented in Fig. 5 as a stacked bar plot. In the following text, results on mixing proportions X_i^E are reported as $D_{50}{}^{+D_{84}}_{-D_{16}}$ (D_n is the nth percentile of the output distribution over the 10 000 simulations; thus, D_{50} is the median).

Carbonate dissolution appears as the major contributor to dissolved Ca and to about half of dissolved Mg in all the springs sampled in the different parts of the studied zone (UZ, BSZ and MSZ), making this process a major supplier of cationic charges to waters at Séchilienne (Table S2; Fig. 5). In the most active part of the landslide (G1, G2), despite the silicate-dominated lithology, the carbonate contribution is significant (about 40 %), indicating that the waters percolating though the unstable zone acquired part of their chemical and isotopic composition from above the hillslope. Calculations of the proportions of sulfate derived from the different end members show a minor but non-negligible contribution of gypsum dissolution (reaching 88 % of the total sulfate in spring S15) and a very clear contribution of pyrite oxidative weathering, which is particularly important in the fractured zone. In the G1–G2–S10 group of springs, most of the anionic charge (> 80 %) is provided by the oxidative weathering of pyrite. Springs from the BSZ exhibit a lower proportion from the silicate end member with a median of $0.48^{0.76}_{0.24}$ against $0.61^{0.84}_{0.38}$ and $0.56^{0.81}_{0.31}$ for G1 and G2 (UZ), respectively. This contrast can be attributed to the unstable context of G1 and G2 compared with that of the stable part of the slope at the BSZ outflow.

Gypsum dissolution is a major process at some sites (with the fraction of SO_4 from gypsum ranging between $0.57^{0.79}_{0.43}$ and $0.88^{0.97}_{0.80}$ in waters of the MSZ, S13–S21, for example), but nowhere does this process dominate the overall solute production (Fig. 5). Therefore, although significant uncertainty exists regarding the S isotope composition of the pyrite

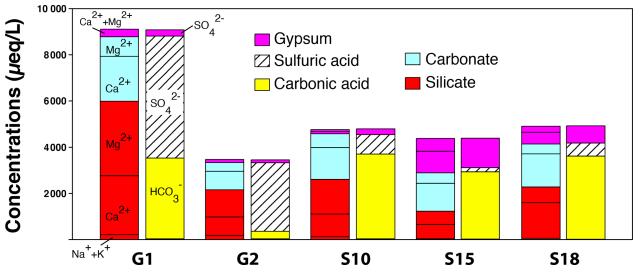

Figure 5. Concentration (in charge equivalents) calculated for major dissolved species and for each end member from the mixing model presented in the text and in the Supplement (Table S2). Silicates contribute Na + K + Ca + Mg (Na + K not indicated), carbonates contribute Ca + Mg and gypsum dissolution contributes Ca + Mg (not distinguished). Note that the hydrogenocarbonate ion ultimately originates from respiration in soils. Sulfuric acid is generated by the oxidation of sulfide minerals, a process that occurs preferentially in the fractured zone. Relative contributions of different end members were obtained by solving a set of mixing equations using a Monte Carlo approach (Sect. 5.1.3). Note that the relative contribution of each rock end member to the Ca^{2+} load here refers to that calculated for the Ca "initially" released into solution – that is, before secondary carbonate precipitation (Supplement).

end member, S isotope data lend support to our inference from the mixing model that waters are derived essentially from pyrite oxidation in the unstable zone and from gypsum dissolution in the MSZ (S13, S15, S18, S20 and S21). The relative contribution of carbonates is also significant in MSZ waters with proportions ranging from $0.32^{0.58}_{0.09}$ for S18 to $0.33^{0.56}_{0.13}$ for S15.

Based on the results of the mixing model, we can estimate a value for $\delta^{34}S$ of the pyrite end member. Indeed, a significant linear negative relationship ($R^2 = 0.8$) exists between the $\delta^{34}S$ measured in springs across the Séchilienne massif and the modal estimates of their $X_{sil}^{SO_4}$ (Fig. S12). The intercept of this relationship at $X_{sil}^{SO_4} = 1$ (equivalently at $X_{gyp}^{SO_4} = 0$) gives an estimate for $\delta^{34}S_{sulfur}$ of −3.1 ‰. Such estimates are consistent with the range of measurements of solid sulfur reported in this study (ranging between −13.1 ‰ and 17.8 ‰) and reflect an average value of the S isotope composition of sulfides for the Séchilienne unstable zone.

5.2 Implications for hydrogeological processes at the Séchilienne site

Water plays an important role in the dynamics of slope instabilities: first, water is a physical (hydrogeological) agent that can lead to aggravation of the instability; second, water is a geochemical agent that weathers rocks and makes them less cohesive (Rutqvist and Stephansson, 2003; Binet, 2006; Cappa et al., 2004). These two categories of processes interact with each other in time as weathering leads to modifications in subsurface permeability and porosity and, thus, in water flow paths through the massif (Gu et al., 2019). Hydro-

logical triggering is the most usual mechanism of initiation and reactivation of landslides, but water flows in the subsurface have also been shown to have a major impact on the destabilization of a slope (de Montety et al., 2007; Guglielmi et al., 2002; Vallet et al., 2015b). However, landslides constitute very heterogeneous media due to their intense fracture formation, which makes hydrogeological investigation complicated. The use of hydrochemistry and isotopic investigation can provide new insight to classical investigation. For example, groundwater dissolved $^{87}Sr / ^{86}Sr$ ratios have proven to be useful in determining the sources of solutes in natural waters (Négrel and Deschamps, 1996; Négrel et al., 2001; Dotsika et al., 2010), investigating mineral weathering reactions (Brass, 1975; Åberg et al., 1989; Bullen et al., 1996; Clow and Drever, 1996; Bullen and Kendall, 1998) and identifying mixing processes involving groundwaters from different sources (Woods et al., 2000; Frost and Toner, 2004; Singleton et al., 2006) as well as in an unstable context (Deiana et al., 2018). Values of groundwater dissolved $\delta^{34}S–SO_4^{2-}$ have also been used in aquifer studies to identify sulfate sources (Moncaster et al., 2000; Cortecci et al., 2002; Gammons et al., 2013). In particular, the Séchilienne hydrogeological model proposed by Vallet et al. (2015a) uses sulfates as a tracer of waters flowing through the instability with the assumption that all SO_4^{2-} measured in groundwaters is sourced from pyrite oxidation. High sulfate concentrations in MSZ waters were indeed inferred by Vallet et al. (2015a) to be derived from a mixture of 30 % of waters from the UZ (drained through the micro-fissured matrix) and 70 % from the sedimentary cover (drained through both micro-fissured matrix and larger fractures), thereby establishing a hydraulic connection between the UZ and the MSZ waters (Fig. 1c).

Results from the present study partly support the hydrogeological model established by Vallet et al. (2015a) but allow us to refine this model through the identification of the contribution of another, unexpected end member corresponding to the dissolution of gypsum with a remote origin. Based on the local geological map (Barféty et al., 1972), gypsum occurrence has been reported but outside of the study zone, upstream along the Sabot Fault which lies to the northeast of the MSZ outflows. As the fault is a major flow path (Lajaunie et al., 2019), draining aquifers hosted by the sedimentary cover to the MSZ outflows, it contributes to the SO_4^{2-} enrichment of those waters (Fig. 6). Therefore, our study indicates a significant evaporitic origin for the sulfates in the MSZ waters, challenging the interpretation of Vallet et al. (2015a) of a hydrogeological connection between waters of the unstable and stable zones. Sulfate in outflows draining the UZ and BSZ is not strongly sourced from evaporites, but the part of those sulfates with evaporitic origin can be explained by a contribution of water flows through the Sabot Fault towards the sedimentary cover and the basement formations (Fig. 6).

In addition, the systematic differences in elemental concentrations observed between the UZ and BSZ outflows (Table 3) can be linked to the structure of the slope and water

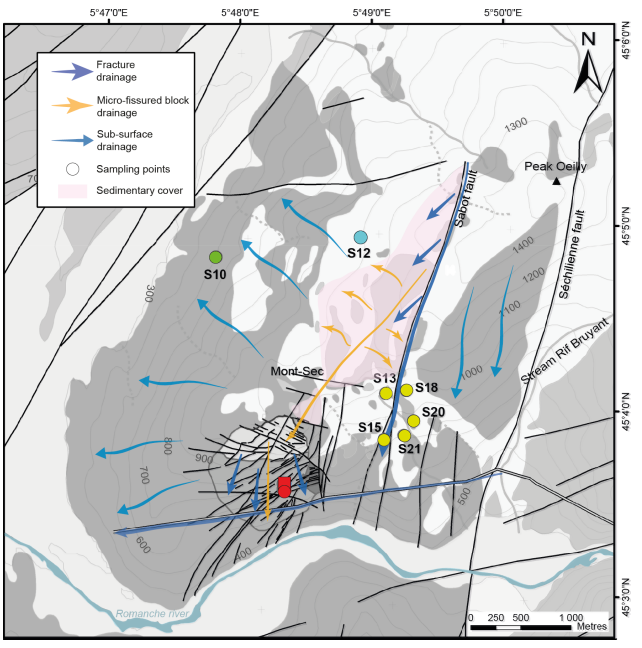

Figure 6. Sketch of the Séchilienne groundwater conceptual model, modified after Vallet et al. (2015).

flow paths in the subsurface. Indeed, the S10 outflow drains a stable area (BSZ) just above the lightly weathered, only slightly fractured basement. By contrast, the G1 and G2 outflows drain the unstable part of the slope (UZ), where the basement is highly fractured. This leads to stronger weathering of rocks and minerals there, in particular of pyrite which is a major contributor to dissolved sulfate in the G1 and G2 outflows – more so than in the S10 outflow (stable and lightly weathered) characterized by lower sulfate contents.

Improving numerical and predictive models requires the incorporation of hydrological processes such as the dynamics of water circulation within a slope (which is directly dependent on factors such as fracturation and the volumes of water involved). This study shows that isotopic proxies such as Sr and S isotopes ($^{87}Sr / ^{86}Sr$, $\delta^{34}S$) coupled with water chemistry can be a very powerful tool to constrain groundwater origin and flow paths in landslides, can act as a substitute for tracer surveys and can constitute an alternative for hydrogeological investigations in logistically challenging field environments such as unstable slopes.

5.3 Role of landslides on silicate weathering and CO_2 consumption

Recent studies have shown the importance of pyrite oxidation, sulfuric acid production and associated chemical weathering in active landslides (Emberson et al., 2015; Emberson et al., 2016). The novelty of the present study is the use of waters sampled within an active, slow landslide, rather than the use of percolation waters sampled at the base of

the colluvium of recent landslides or of river waters draining landslide-affected watersheds. In the following paragraph, we examine the potential implications of the present study of the Séchilienne landslide for the global carbon cycle.

Silicate weathering by carbonic acid consumes atmospheric CO_2 and, combined with the precipitation of carbonates in the ocean, is the mechanism that has allowed for the sequestration of atmospheric CO_2 and has consequently lowered the Earth's surface temperature on geological timescales (Berner and Berner, 2012). Rock-forming minerals uplifted to the Earth's surface react with oxygen, carbonic acid produced by soil respiration and sulfuric acid produced by the oxidation of sulfide minerals. The following reactions describe how carbonic (Eqs. 9 and 11) and sulfuric (Eqs. 10 and 12) acids interact with silicate (here, wollastonite $CaSiO_3$) and carbonate minerals, leading to the production of alkalinity (here, HCO_3^-):

$$CaSiO_3 + 2CO_2 + H_2O \rightarrow SiO_2 + Ca^{2+} + 2HCO_3^- \quad (9)$$

$$CaSiO_3 + H_2SO_4 \rightarrow SiO_2 + H_2O + Ca^{2+} + SO_4^{2-} \quad (10)$$

$$CaCO_3 + CO_2 + H_2O \rightarrow Ca^{2+} + 2HCO_3^- \quad (11)$$

$$2CaCO_3 + H_2SO_4 \rightarrow 2Ca^{2+} + 2HCO_3^- + SO_4^{2-}. \quad (12)$$

It is usually considered that when Ca^{2+} reaches the ocean, over a time period longer than 0.1 to 1 Myr, the precipitation of $CaCO_3$ releases CO_2 into the ocean–atmosphere system according to the following reaction:

$$Ca^{2+} + 2HCO_3^- \leftrightarrow CaCO_3 + CO_2 + H_2O. \quad (13)$$

The influence of the above reactions (Eqs. 9–13) on atmospheric CO_2 partial pressure depends on the timescale considered (Torres et al., 2016). At short timescales (typically $< 10^5$ years), the chemistry of river discharge is able to influence the carbonate system in the ocean. Indeed, the delivery of alkalinity and dissolved inorganic carbon (DIC) to the ocean to a ratio lower than that of the modern seawater ratio (Alk/DIC ~ 1) leads to an increased dissolved CO_2 concentration and, in turn, a higher CO_2 content in the atmosphere through re-equilibration (Zeebe and Wolf-Gladrow, 2001). If the Alk / DIC ratio is higher than 1 but lower than 2, at timescales longer than that typical of carbonate precipitation in the ocean (10^5 to 10^6 years) but shorter than that of marine sulfate reduction to sulfide in sea-bottom sediments (several 10^6 years), atmospheric CO_2 will increase because the precipitation of carbonates releases CO_2 to the ocean–atmosphere system that was not consumed on land by weathering reactions (combination of Eqs. 12 and 13). This mechanism should lead to global warming (Calmels et al., 2007) and has been invoked by Torres et al. (2014) for maintaining atmospheric CO_2 levels during the Himalayan orogeny, which otherwise should have led to a rapid atmospheric CO_2 depletion by enhanced silicate weathering. Finally, at timescales longer than that typical of the sedimentary burial of sulfide in the ocean, only silicate weathering by carbonic acid leads to net C sequestration (Berner and Berner, 1996; Calmels et al., 2007).

However, our analysis demonstrates that Reaction (13) also occurs directly on the continent at Séchilienne through the formation of secondary carbonates, favored by the addition of calcium and alkalinity derived from silicate weathering, which results in a "shortcut" of the carbon cycle. This short-term CO_2 release has to be taken into account when evaluating the overall CO_2 effect of weathering reactions at Séchilienne as well as more generally in lithologically complex weathering systems where secondary carbonate formation is likely to involve solutes produced by a variety of processes, in particular by carbonate weathering by sulfuric acid.

To this aim, we use the stoichiometry of Eqs. (9) to (13) and the results of our quantitative source apportionment (Sect. 5.1.4) to calculate the impact of weathering reactions at Séchilienne on atmospheric CO_2 over two scales (convoluted spatially and temporally), referred to in the following as "on site" or "local" (i.e., immediately when weathering processes take place in the unstable zone) and "long term" or "global" (i.e., taking marine carbonate precipitation in the ocean ensuing solute delivery to the ocean into account).

Figure 7 shows that waters produced in the unstable zone of Séchilienne (G1 and G2) act as CO_2 sources in the long term, whereas waters produced in the bedrock stable zone (S10) or the mixed stable zone (S15, S18) are CO_2 sinks or CO_2-neutral within uncertainty. Thus, our study shows that instabilities such as the Séchilienne landslide can act as hotspots of long-term CO_2 release to the atmosphere depending on the types of mineral–fluid interactions and also on the flow paths followed by the water drained in the landslide. We suggest that chemical weathering in similar landslides throughout the Alps (i.e., Clapière, Super Sauze and Valabres in the French Alps and Rosone in Italy; Barla and Chiriotti, 1995; Follacci, 1999; Binet, 2006) have a similar impact on global biogeochemical cycles and climate. Although it is beyond the scope of the present study to quantify the CO_2 fluxes linked to weathering in the Séchilienne landslide – let alone to attempt an extrapolation of such local results to the scale of the Alpine range – our work clearly shows that silicate and carbonate weathering by sulfuric acid generated in landslide zones of active mountain ranges have a climatic impact though a complex set of entangled short-term and long-term effects. Furthermore, this impact contradicts the textbook view that silicate weathering in mountain ranges consumes CO_2 from the atmosphere and cools the global climate (Raymo, 1991; Hilton and West, 2020), and it motivates more detailed studies associating hydrogeological and mineralogical approaches in order to build a more realistic understanding of the impact of mountains on climate change.

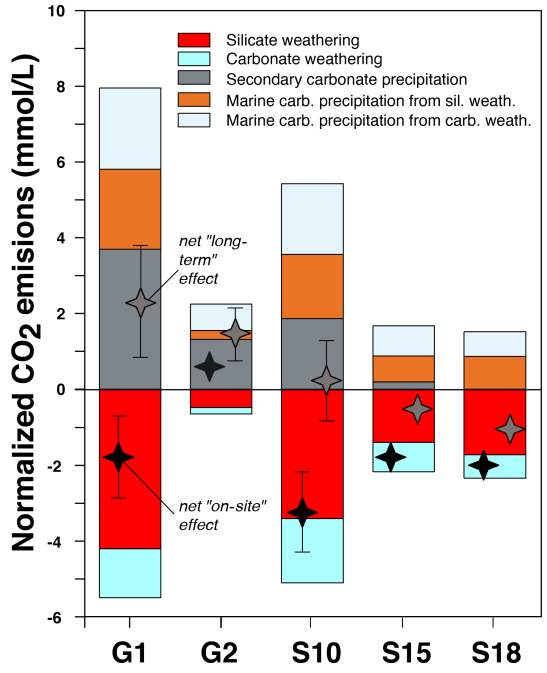

Figure 7. Evaluation of the effect of weathering processes at Séchilienne on atmospheric CO_2. The hydrochemistry of the G1 and G2 springs draining the instability (the unstable zone) show that the weathering results in long-term CO_2 production to the atmosphere because the cations are preferentially released in spring waters by the action of sulfuric acid and not carbonic acid from the soils (Table S3 in the Supplement). In the bedrock stable zone (spring S10) and in the mixed stable zone (springs S15 and S18), weathering processes act as CO_2 sinks or are CO_2-neutral within uncertainty. Secondary carbonate precipitation returns CO_2 to the atmosphere. In particular, in the G2 spring of the unstable zone, this process results in a net "on-site" CO_2 release because it involves precipitation of Ca and alkalinity derived from carbonate weathering by sulfuric acid.

6 Conclusion

We use measurements of dissolved major element chemistry coupled to Sr and S isotopic ratios in spring waters of the Séchilienne active landslide site in order to identify the chemical processes at play in the subsurface of the landslide area. Among these tracers, strontium isotopes allow us to allocate cations to different sources, circumventing issues affecting elemental ratios related to the precipitation of secondary carbonate. Silicate, carbonate and evaporite weathering all appear to contribute to the cation load of the Séchilienne waters. Scavenging of dissolved calcium by secondary carbonate formation is identified as a major process affecting solutes in the subsurface waters of the Séchilienne instability and is favored by the mixing of different solutions that have interacted with a heterogeneous set of minerals. Sulfur isotopes provide a unique qualitative constraint on the origin of the sulfate ion, which is abundant in the Séchilienne groundwaters, showing the contribution of not only pyrite oxidation but also of gypsum dissolution.

The provenance of dissolved species at Séchilienne also reveals the complex water flow paths there. In particular, waters percolating through the landslide have acquired part of their hydrochemical characteristics far away from the unstable zone itself. For example, sulfur isotopes clearly indicate an unexpected contribution from Triassic sedimentary gypsum dissolution, which can only occur in the sedimentary layers capping the upper part of the massif; this emphasizes the importance of water drainage by a major fault of the massif.

The comparison between the stable and unstable parts of the site suggests that silicate weathering is enhanced in the fractured, unstable zone, where the landslide is active. Sulfur isotopes indicate that the production of acidity by the oxidation of magmatic sulfides enhances rock alteration in the unstable zone. This leads us to suggest the following feedback. By favoring the penetration of oxic waters and allowing contact with silicate minerals, fracture formation and grain comminution controls the oxidation of pyrite that, in turn, rapidly generates sulfuric acid. The weathering of silicate minerals by sulfuric acid weakens the rock structure, and this favors fracturation in response to the gravitational stress. For example, Fletcher et al. (2006) and Behrens et al. (2015) have shown that the opening of porosity at the rock–soil interface in soil profiles can be initiated by the oxidation of Fe(II) minerals, inducing a positive volume budget and leading to the production of micro-cracks, causing further weathering, at the origin of the opening of fractures, provided that enough carbonate and pyrite are present in the bedrock. At a larger scale, the feedback that we propose here exemplifies a similar process of coupling between physical and chemical processes sustaining mass wasting in mountain ranges.

Finally, we demonstrate that the Séchilienne landslide is a hotspot of CO_2 release to the atmosphere over the long term. Although it remains difficult to upscale the results of the present study to the entire Alpine range (or to a global scale), landslides developed on sulfide-hosting sedimentary rocks appear to have a climatic impact opposite to the conventional view that rock weathering in mountain ranges consumes CO_2 from the atmosphere and, thus, contributes to global cooling. In addition, our study shows a strong control of weathering processes and rates by local hydrogeological features, such as the complexity of flow paths setting the chemistry of the groundwaters within the unstable zone. More work is needed to assess the importance of landslides as hotspots of chemical alteration and geological CO_2 emissions, in particular to investigate their hydrological and hydrochemical response to weather and climate change. More generally, landslides epitomize the coupling between landscape evolution, tectonics, and climate and weather. For this reason – as well as their societal impact in terms of natural hazard – monitoring landslides over a range of timescales and frequency should become a priority.

Code availability. The code used in this study to solve the geochemical mixing model and to produce some of the plots is published under the https://doi.org/10.5281/zenodo.4779121 (Bouchez et al., 2021).

Data availability. All relevant data are available at https://doi.org/10.5281/zenodo.4606732 (Nevers et al., 2021).

Supplement. The supplement related to this article is available online at: https://doi.org/10.5194/esurf-9-487-2021-supplement.

Author contributions. PN measured the Sr isotopic ratios, worked on the interpretation and wrote the text. JB and JG helped with the isotopic measurements, the inversion calculations and writing the text. CT measured the sulfur isotopic ratios. DC worked on the XRD and mineralogic analyses presented in the Supplement. LF helped with the rock sample leaching procedure and Sr isotope measurements. CB organized the sampling strategy, is in charge of the Séchilienne Observatory (SNO OMIV) and helped with writing the text.

Competing interests. The authors declare that they have no conflict of interest.

Acknowledgements. Part of this work was supported by the IPGP multidisciplinary "PARI" program and by the Region île-de-France "SESAME" program (grant no. 12015908). Caroline Gorge, Christophe Loup and Caroline Amiot are acknowledged for analytical support, and Vanessa Stefani is acknowledged for support on the field. The authors warmly thank the PEA^{2}t platform (Chrono-Environment, University of Burgundy, University of Franche-Comté, UMR CNRS 6249, France), which manages and maintains the analytical equipment used in this study, and OMIV and OSU Theta for supporting the project through financial contributions (SRO_2015).

Financial support. This project has been supported by OSU THETA (Observatory of Sciences of the Universe), SRO 2017 (OSU Research Support), and the INSU (National Institute of Sciences of the Universe) project, EC2CO 2018.

Review statement. This paper was edited by Robert Hilton and reviewed by Xin Gu.

References

Åberg, G., Jacks, G., Hamilton, P. J.: Weathering rates and ^{87}Sr / ^{86}Sr ratios: An isotopic approach, J. Hydrol., 109, 65–78, https://doi.org/10.1016/0022-1694(89)90007-3, 1989.

Balci, N., Mayer, B., Shanks, W. C., and Mandernack, K. W.: Oxygen and sulfur isotope systematics of sulfate produced during abiotic and bacterial oxidation of sphalerite and elemental sulfur, Geochim. Cosmochim. Ac., 77, 335–351, https://doi.org/10.1016/j.gca.2011.10.022, 2012.

Barféty, J., Bordet, P., Carme, F., Debelmas, J., Meloux, M., Montjuvent, G., and Sarrot Reynauld, J.: Carte géologique détaillée de la France (1/50 000) no. 797 Vizille, Editions du BRGM, p. 38, 1972.

Barla, G. and Chiriotti, E.: Insights into the behaviours of the large deep seat gravitational slope deformation of Rosone, in the Piemont region (Italy), Felsbau, 13, 425–432, 1995.

Barnes, H. L. (Ed.): Geochemistry of hydrothermal ore deposits, John Wiley & Sons, New-York, Chichester, Weinheim, Brisbane, Singapore, Toronto, 1997.

Baudement, C., Bertrand, C., Guglielmi, Y., Viseur, S., Vallet, A., and Cappa, F.: Quantification de la dégradation mécanique et chimique d'un versant instable: approche géologique, hydromécanique et hydrochimique: Etude du versant instable de Séchilienne, Isère (38), JAG – 3e journees des aleas gravitaires, France, 1–6, 2013.

Behrens, R., Bouchez, J., Schuessler, J. A., Dultz, S., Hewawasam, T., and von Blanckenburg, F.: Mineralogical transformations set slow weathering rates in low-porosity metamorphic bedrock on mountain slopes in a tropical climate, Chem. Geol., 411, 283–298, https://doi.org/10.1016/j.chemgeo.2015.07.008, 2015.

Berner, E. K. and Berner, R. A.: Global Environment: Water, Air, and Geochemical Cycles. Upper Saddle River, New Jersey, Prentice Hall, Inc., 376 pp., 1996.

Berner, K. E. and Berner, R. A.: Global Environment: Water, Air and Geochemical Cycles, Princeton Univ. Press, USA, 369–382, 2012.

Bertrand, C., Vallet, A., and Mudry, J.: Hydrochemical Approach of Mechanical Degradation of the Séchilienne Unstable Slope, in: Engineering Geology for Society and Territory – Volume 2, edited by: Lollino, G., Giordan, Crosta, G. B., Corominas, J., Azzam, R., Wasowski, J., and Sciarra, N., Springer International Publishing Switzerland, chap. 383, https://doi.org/10.1007/978-3-319-09057-3_383, 2015.

Bickle, M. J., Tipper, E. T., Galy, A., Chapman, H., and Harris, N.: On Discrimination Between Carbonate and Silicate Inputs to Himalayan Rivers, Am. J. Sci., 315, 120–166, https://doi.org/10.2475/02.2015.02, 2015.

Binet, S.: L'hydrochimie, marqueur de l'évolution à long terme des versant montagneux fracturés vers de grands mouvements de terrain: application à plusieurs échelles sur la haute vallée de la Tinée (Mercantour, France) et sur le versant de Rosone (Gran Paradiso, Italie), PhD Thesis Université de Franche-Comté, Besançon, 2006.

Binet, S., Spadini, L., Bertrand, C., Guglielmi, Y., Mudry, J., and Scavia, C.: Variability of the groundwater sulfate concentration in fractured rock slopes: a tool to identify active unstable areas, Hydrol. Earth Syst. Sci., 13, 2315–2327, https://doi.org/10.5194/hess-13-2315-2009, 2009.

Blattmann T. M., Wang, S. L., Lupker, M., Märki, L., Haghipour, N., Wacker, L., Chung, L. H., Bernasconi, S. M., Plötze, M., and Eglinton, T. I.: Sulphuric acid-mediated weathering on Taiwan buffers geological atmospheric carbon sinks, Sci. Rep.-UK, 9, 2945, https://doi.org/10.1038/s41598-019-39272-5, 2019.

Bouchez, J., Nevers, P., Gaillardet, J., and Bertrand, C.: Numerical code for solving the geochemical mixing model and making diagrams in Nevers et al., to be published in E-surf ("Landslides as geological hotspots of CO_2 to the atmosphere: clues from the instrumented Séchilienne landslide, Western European Alps") (Version Corresponds to the published version of the article (final)), Zenodo, https://doi.org/10.5281/zenodo.4779121, 2021.

Brass, G. W.: The effect of weathering on the distribution of strontium isotopes in weathering profiles, Geochim. Cosmochim. Ac., 39, 1647–1653, https://doi.org/10.1016/0016-7037(75)90086-1, 1975.

Bullen, T. D., Krabbenhoft, D. P., and Kendall, C.: Kinetic and mineralogic controls on the evolution of groundwater chemistry and $^{87}Sr/^{86}Sr$ in a sandy silicate aquifer, northern Wisconsin, USA, Geochim. Cosmochim. Ac., 60, 1807–1821, https://doi.org/10.1016/0016-7037(96)00052-X, 1996.

Bullen, T. D. and Kendall, C.: Tracing of Weathering Reactions and Water Flowpaths: A Multi-isotope Approach, in: Isotope Tracers in Catchment Hydrology, edited by: Kendall, C. and McDonnell, J. J., Elsevier Science B.V., Amsterdam, 611–646, https://doi.org/10.1016/B978-0-444-81546-0.50025-2, 1998.

Burke, W. H., Denison, R. E., Hetherington, E. A., Koepnick, R. B., Nelson, H. F., and Otto, J. B.: Variation of seawater $^{87}Sr/^{86}Sr$ throughout Phanerozoic time, Geology, 10, 516–519, https://doi.org/10.1130/0091-7613(1982)10<516:VOSSTP>2.0.CO;2, 1982

Calmels, D., Gaillardet, J., Brenot, A., and France-Lanord, C.: Sustained sulfide oxidation by physical erosion processes in the Mackenzie River basin: Climatic perspectives, Geology, 35, 1003–1006, https://doi.org/10.1130/G24132A.1, 2007.

Canfield, D. E., Raiswell, R., Westrich, J. T., Reaves, C. M., and Berner, R. A.: the use of chromium reduction in the analysis of reduced inorganic sulfur in sediments and shales, Chem. Geol., 54, 149–155, https://doi.org/10.1016/0009-2541(86)90078-1, 1986.

Cappa, F., Guglielmi, Y., Soukatchoff, V., Mudry, J., Bertrand, C., and Charmoille, A.: Hydromechanical modeling of a large moving rock slope inferred from slope levelling coupled to spring long-term hydrochemical monitoring: example of the La Clapière landslide (Southern Alps, France), J. Hydrol., 291, 67–90, https://doi.org/10.1016/J.JHYDROL.2003.12.013, 2004.

Clow, D. W. and Drever, J. I.: Weathering rates as a function of flow through an alpine soil, Chem. Geol., 132, 131–141, https://doi.org/10.1016/S0009-2541(96)00048-4, 1996.

Cortecci, G., Dinelli, E., Bencini, A., Adorni-Braccesi, A., and La Ruffa, G.: Natural and anthropogenic SO_4 sources in the Arno river catchment, northern Tuscany, Italy: a chemical and isotopic reconnaissance, Appl. Geochem., 17, 79–92, https://doi.org/10.1016/S0883-2927(01)00100-7, 2002.

Deiana, M., Cervi, F., Pennisi, M., Mussi, M., Bertrand, C., Tazioli, A., and Ronchetti, F.: Chemical and isotopic investigations (δ18O, δ2H, 3H, $^{87}Sr/^{86}Sr$) to define groundwater processes occurring in a deep-seated landslide in flysch. Hydrogeol. J., 26, 2669–2691, https://doi.org/10.1007/s10040-018-1807-1, 2018.

Dotsika, E., Poutoukis, D., Kloppmann, W., Guerrot, C., Voutsa, D., and Kouimtzis, T. H.: The use of O, H, B, Sr and S isotopes for tracing the origin of dissolved boron in groundwater in Central Macedonia, Greece, Appl. Geochem., 25, 1783–1796, https://doi.org/10.1016/J.APGEOCHEM.2010.09.006, 2010.

Dubois, L., Chanut, M.-A., and Duranthon, J. P.: Amélioration continue des dispositifs d'auscultation et de surveillance integrés dans le suivi du versant instable des Ruines de Séchilienne in: Géologues, 182, edited by: Editions du BRGM, 50–55, 2014.

Emberson, R., Hovius, N., Galy, A., and Marc, O.: Chemical weathering in active mountain belts controlled by stochastic bedrock landsliding, Nat. Geosci., 9, 42–45, https://doi.org/10.1038/ngeo2600, 2015.

Emberson, R., Hovius, N., Galy, A., and Marc, O.: Oxidation of sulfides and rapid weathering in recent landslides, Earth Surf. Dynam., 4, 727–742, https://doi.org/10.5194/esurf-4-727-2016, 2016b.

Emberson, R., Galy, A., and Hovius, N.: Weathering of Reactive Mineral Phases in Landslides Acts as a Source of Carbon Dioxide in Mountain Belts, J. Geophys. Res.-Earth, 123, 2695–2713. https://doi.org/10.1029/2018JF004672, 2018.

Fanlo, I. and Ayora, C.: The evolution of the Lorraine evaporitic basin: implications for the chemical and isotope composition of the Triassic ocean, Chem. Geol., 146, 135–154, 1998.

Fletcher, R. C., Buss, H. L., and Brantley, S. L.: A spheroidal weathering model coupling porewater chemistry to soil thicknesses during steady-state denudation, Earth Planet. Sc. Lett., 244, 444–457, https://doi.org/10.1016/j.epsl.2006.01.055, 2006.

Follacci, J.: Seize ans de surveillance du glissement de la Clapière (Alpes maritimes), 220, Rapport, Bulletin du Laboratoire des Ponts et Chaussés, 220, 35–51, 1999.

Frost, C. D. and Toner, R. N.: Strontium isotopic identification of water-rock interaction and ground water mixing, Ground Water, 42, 418–432, https://doi.org/10.1111/j.1745-6584.2004.tb02689.x, 2004.

Fry, B., Cox, J., Gest, H., and Hayes J. M.: Discrimination between 34S and 32S during bacterial metabolism of inorganic sulfur compounds, J Bacteriol., 165, 328–330, https://doi.org/10.1128/jb.165.1.328-330.1986, 1986.

Fry, B., Ruf, W., Gest, H., and Hayes, J. M.: Sulfur isotope effects associated with oxidation of sulfide by O_2 in aqueous solution, Chem. Geol., 73, 205–210, https://doi.org/10.1016/0168-9622(88)90001-2, 1988.

Gaillardet, J., Dupre, B., Allegre C. J., and Négrel, P.: Chemical and physical denudation in the Amazon River Basin, Chem. Geol., 142, 141–173, https://doi.org/10.1016/S0009-2541(97)00074-0, 1997.

Gaillardet, J., Dupre, B., Louvat, P., and Allegre, C. J.: Global silicate weathering and CO_2 consumption rates deduced from the chemistry of large rivers, Chem. Geol., 159, 3–30, https://doi.org/10.1016/S0009-2541(99)00031-5, 1999.

Gammons, C. H., Brown, A., Poulson, S. R., and Henderson, T. H.: Using stable isotopes (S, O) of sulfate to track local contamination of the Madison karst aquifer, Montana, from abandoned coal mine drainage, Appl. Geochem., 31, 228–238, https://doi.org/10.1016/J.APGEOCHEM.2013.01.008, 2013.

Gu, X., Rempe, D., Dietrich, W., West, A., Lin, T. C., Jin, L., and Brantley, S.: Chemical reactions, porosity, and microfracturing in shale during weathering: The effect of erosion rate, Geochim. Cosmochim. Ac., 269, 63–100, https://doi.org/10.1016/j.gca.2019.09.044, 2019.

Guglielmi, Y., Vengeon, J., Bertrand, C., Mudry, J., Follacci, J., and Giraud, A.: Hydrogeochemistry: an investigation tool to evaluate infiltration into large moving rock masses (case study of La

Clapière and Séchilienne alpine landslides), B. Eng. Geol. Environ., 61, 311–324, https://doi.org/10.1007/s10064-001-0144-z, 2002.

Hajj, F., Poszwa, A., Bouchez, J., and Guérold, F.: Radiogenic and "stable" strontium isotopes in provenance studies: A review and first results on archaeological wood from shipwrecks, J. Archaeol. Sci., 86, 24–49, https://doi.org/10.1016/j.jas.2017.09.005, 2017.

Hilton, R. G. and West, A. J.: Mountains, erosion and the carbon cycle, Nature Reviews Earth & Environment, 1, 284–299, https://doi.org/10.1038/s43017-020-0058-6, 2020.

Kampschulte, A. and Strauss, H.: The sulfur isotopic evolution of Phanerozoic seawater based on the analysis of structurally substituted sulfate in carbonates, Chem. Geol., 204, 255–286, https://doi.org/10.1016/j.chemgeo.2003.11.013, 2004.

Koepnick, R. B., Denison, R. E., Burke, W. H., Hetherington, E. A., and Dahl, D. A.: Construction of the Triassic and Jurassic portion of the Phanerozoic curve of seawater $^{87}Sr/^{86}Sr$, Chem. Geol., 80, 327–349, https://doi.org/10.1016/0168-9622(90)90014-4, 1990.

Lajaunie, M., Gance, J., Nevers, P., Malet, J.-P., Bertrand, C., Garin, T., and Ferhat, G.: Structure of the Seìchilienne unstable slope from large-scale 3d electrical tomography using a resistivity distributed automated system (r-das), Geophys. J. Int., 219, 129–147, https://doi.org/10.1093/gji/ggz259, 2019.

Lasaga, A. C.: Chemical kinetics of water-rock interactions, J. Geophys. Res.-Sol. Ea., 89, 4009–4025, https://doi.org/10.1029/jb089ib06p04009, 1984.

Lerman, A., Wu, L., and Mackenzie, F. T.: CO_2 and H_2SO_4 consumption in weathering and material transport to the ocean, and their role in the global carbon balance, Mar. Chem., 106, 326–350, https://doi.org/10.1016/j.marchem.2006.04.004, 2007.

Le Roux, O., Jongmans, D., Kasperski, J., Schwartz, S., Potherat, P., Lebrouc, V., and Meric, O.: Deep geophysical investigation of the large Séchilienne landslide (Western Alps, France) and calibration with geological data, Eng. Geol., 120, 18–31, https://doi.org/10.1016/J.ENGGEO.2011.03.004, 2011.

Li, S. L., Calmels, D., Hana, G., Gaillardet, J., and Liu, C. Q.: Sulfuric acid as an agent of carbonate weathering constrained by δ^{13}CDIC: Examples from Southwest China, Earth Planet. Sc. Lett., 270, 3–4, 189–199, https://doi.org/10.1016/j.epsl.2008.02.039, 2008.

Maréchal, J.-C.: Les circulations d'eau dans les massifs cristallins alpins et leurs relations avec les ouvrages souterrains. PhD Thesis, Ecole Polytechnique Fédérale de Lausanne (EPFL), Suisse, 1998.

Meric, O., Garambois, S., Jongmans, D., Wathelet, M., Chatelain, J. L., and Vengeon, J. M.: Application of geophysical methods for the investigation of the large gravitational mass movement of Séchilienne, France, Can. Geotech. J., 42, 1105–1115, https://doi.org/10.1139/t05-034, 2005.

Meybeck, M.: Composition chimique des ruisseaux non pollués en France, Chemical composition of headwater streams in France, Sciences Géologiques, 39, 3–77, https://doi.org/10.3406/sgeol.1986.1719, 1986.

Meynadier, L., Gorge, C., Birck, J., and Allègre, C.: Automated separation of Sr from natural water samples or carbonate rocks by high performance ion chromatography, Chem. Geol., 227, 26–36, https://doi.org/10.1016/j.chemgeo.2005.05.012, 2006.

Moncaster, S. J., Bottrell, S. H., Tellam, J. H., Lloyd, J. W., and Konhauser, K. O.: Migration and attenuation of agrochemical pollutants: Insights from isotopic analysis of groundwater sulphate, J. Contam. Hydrol., 43, 147–163, https://doi.org/10.1016/S0169-7722(99)00104-7, 2000.

Montety, V. de, Marc, V., Emblanch, C., Malet, J.-P., Bertrand, C., Maquaire, O., and Bogaard, T. A.: Identifying the origin of groundwater and flow processes in complex landslides affecting black marls: insights from a hydrochemical survey, Earth Surf. Proc. Land., 32, 32–48, https://doi.org/10.1002/esp.1370, 2007.

Montjuvent, G. and Winistorfer, J.: Glaciations quaternaires dans les Alpes franco-suisses et leur piedmont, Géologie Alpine, 56, 251–282, 1980.

Mudry, J. and Etievant, K.: Synthese hydrogéologique du versant instable des Ruines de Séchilienne, Unpublished report, UMR Chrono-Environnement, University of Franche-Comteì, Besançon, 2007.

Négrel, P., Allègre, C. J., Dupré, B., and Lewin, E.: Erosion sources determined by inversion of major and trace element ratios and strontium isotopic ratios in river: The Congo Basin case, Earth Planet. Sc. Lett., 120, 59–76, https://doi.org/10.1016/0012-821X(93)90023-3, 1993.

Négrel, P. and Deschamps, P.: Natural and anthropogenic budgets of a small watershed in the massif central (France): Chemical and strontium isotopic characterization of water and sediments, Aquat. Geochem., 2, 1–27, https://doi.org/10.1007/BF00240851, 1996.

Négrel, P., Casanova, J., and Aranyossy, J.-F.: Strontium isotope systematics used to decipher the origin of groundwaters sampled from granitoids: the Vienne Case (France), Chem. Geol., 177, 287–308, https://doi.org/10.1016/S0009-2541(00)00414-9, 2001.

Nevers, P., Bouchez, J., Gaillardet, J., Thomazo, C., Faure, L., and Bertrand, C.: Dataset of Nevers et al. in E-surf Discussions: "Landslides as geological hotspots of CO_2 to the atmosphere: clues from the instrumented Séchilienne landslide, Western European Alps" (doi:10.5194/esurf-2020-42) [Data set], Zenodo, https://doi.org/10.5281/zenodo.4606732, 2021.

Oudin, L., Hervieu, F., Michel, C., Perrin, C., Andreìassian, V., Anctil, F., and Loumagne, C.: Which potential evapotranspiration input for a lumped rainfall–runoff model?: Part 2 – towards a simple and efficient potential evapotranspiration model for rainfall–runoff modelling, J. Hydrol., 303, 290–306, 2005.

Potherat, P. and Alfonsi, P.: Les mouvements de versant de Séchilienne (Isère). Prise en compte de Thériatage structural pour leur simulation numérique, Rev. Fr. Géotech., 95–96, 117–131, https://doi.org/10.1051/geotech/2001095117, 2001.

Raymo, M. E.: Geochemical evidence supporting T. C. Chamberlin's theory of glaciation, Geology, 19, 344–347, https://doi.org/10.1130/0091-7613(1991)019<0344:GESTCC>2.3.CO;2, 1991.

Raymo, M. and Ruddiman, W.: Tectonic forcing of late Cenozoic climate, Nature, 359, 117–122, https://doi.org/10.1038/359117a0, 1992.

Rutqvist, J. and Stephansson, O.: The role of hydromechanical coupling in fractured rock engineering, Hydrogeol. J., 11, 7–46, https://doi.org/10.1007/s10040-002-0241-5, 2003.

Singleton, M. J., Maher, K., DePaolo, D. J., Conrad, M. E., and Evan Dresel, P.: Dissolution rates and vadose zone drainage

from strontium isotope measurements of groundwater in the Pasco Basin, WA unconfined aquifer, J. Hydrol., 321, 39–58, https://doi.org/10.1016/J.JHYDROL.2005.07.044, 2006.

Spence, J. and Telmer, K.: The role of sulfur in chemical weathering and atmospheric CO_2 fluxes: evidence from major ions, δ^{13}CDIC, and δ^{34}S SO_4 in rivers of the Canadian Cordillera, Geochimica Cosmochem. Ac., 69, 5441–5458, https://doi.org/10.1016/j.gca.2005.07.011, 2005.

Stallard, R. F. and Edmond, J. M.: Geochemistry of the Amazon: 2. The influence of geology and weathering environment on the dissolved load, J. Geophys. Res.-Oceans, 88, 9671–9688, https://doi.org/10.1029/jc088ic14p09671, 1983.

Tessier, A., Campbell, P. G. C., and Bisson, M.: Sequential extraction procedure for the speciation of particulate trace metals, Anal. Chem., 51, 844–851, https://doi.org/10.1021/ac50043a017, 1979.

Torres, M. A., West, A. J., and Li, G.: Sulphide oxidation and carbonate dissolution as a source of CO_2 over geological timescales, Nature, 507, 346–349, https://doi.org/10.1038/nature13030, 2014.

Torres, M. A., West, A. J., Clark, K. E., Paris, G., Bouchez, J., Ponton, C., and Adkins, J. F.: The acid and alkalinity budgets of weathering in the Andes–Amazon system: Insights into the erosional control of global biogeochemical cycles, Earth Planet. Sc. Lett., 450, 381–391, https://doi.org/10.1016/j.epsl.2016.06.012, 2016.

Vallet, A.: Mouvements de fluides et processus de déstabilisation des versants alpins: Apport de l'étude de l'instabilité de Séchilienne, PhD Thesis, Université de Franche-Comté, Besançon, 2014.

Vallet, A., Bertrand, C., Mudry, J., Bogaard, T., Fabbri, O., Baudement, C., and Régent, B.: Contribution of time-related environmental tracing combined with tracer tests for characterization of a groundwater conceptual model: a case study at the Séchilienne landslide, western Alps (France), Hydrogeol. J., 23, 1761–1779, https://doi.org/10.1007/s10040-015-1298-2, 2015a.

Vallet, A., Charlier, J. B., Fabbri, O., Bertrand, C., Carry, N., and Mudry, J.: Functioning and precipitation-displacement modelling of rainfall-induced deep-seated landslides subject to creep deformation, Landslides, 13, 653–670, https://doi.org/10.1007/s10346-015-0592-3, 2015b.

Vengeon, J. M.: Déformation et rupture des versants en terrain métamorphique anisotrope : Apport de l'étude des Ruines de Séchilienne, PhD Thesis, Université Joseph-Fourier – Grenoble I, 1998

Vengeon, J.-M., Couturier, B., and Antoine, P.: Déformations gravitaires post glaciaires en terrains métamorphiques. Comparaison des indices de déformation du versant sud de la Toura (Saint-Christophe-en-Oisans, France) avec le phénomène de rupture interne du versant sud du Mont Sec (Séchilienne, France), B. Eng. Geol. Environ., 57, 387–395, https://doi.org/10.1007/s100640050062, 1999.

Woods, T. L., Fullagar, P. D., Spruill, R. K., and Sutton, L. C.: Strontium isotopes and major elements as tracers of ground water evolution: example from the Upper Castle Hayne Aquifer of North Carolina, Ground Water, 38, 762–771, https://doi.org/10.1111/j.1745-6584.2000.tb02712.x, 2000.

Zeebe, R. E. and Wolf-Gladrow, D. A.: CO_2 in Seawater: Equilibrium, Kinetics, Isotopes, Elsevier Oceanography Series, Amsterdam, 65, 360 pp., 2001.

Zerkle, A. L., Farquhar, J., Johnston, D. T., Cox, R. P., and Canfield, D. E.: Fractionation of Multiple Sulfur Isotopes During Phototrophic Oxidation of Sulfide and Elemental Sulfur by a Green Sulfur Bacterium, Geochim. Cosmochim. Ac., 73, 291–306, https://doi.org/10.1016/j.gca.2008.10.027, 2009